

**CATALYST COATED MEMBRANES (CCMs) FOR POLYMER  
ELECTROLYTE MEMBRANE (PEM) FUEL CELLS**

by

**Olivia Barron**



Submitted in fulfilment of the requirements for the degree of

Masters in Chemistry

Department of Chemistry,

University of the Western Cape

Supervisor: Dr. Shan Ji

November 2010

## Declaration

I declare that “Catalyst coated membranes (CCMs) for Polymer Electrolyte Membrane (PEM) fuel cells.” is my own work and that it has not been submitted for any degree or examination in any other university, and that all the sources that I have used or quoted have been indicated and acknowledged by complete references

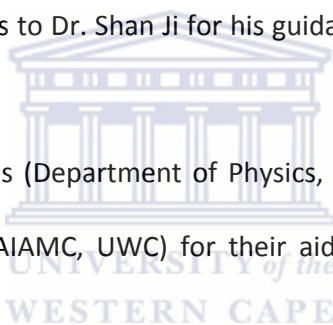
Olivia Barron

November, 2010

Signed.....

## Acknowledgements

- I firstly thank our Lord God for his love and grace that I have experienced and for all the advantages he has provided me with in my life
- I thank my family for their love, support, and encouragement without which I would never have been able to stay motivated throughout the duration of the research
- I am profoundly grateful to Prof. Vladimir Linkov and the staff at the South African Institute for Advanced Material Chemistry (SAIAMC) for allowing me to conduct my research, as well as for financial support
- A special thank you also goes to Dr. Shan Ji for his guidance and support throughout the duration of the research
- Thank you to Adrian Josephs (Department of Physics, UWC), Wafeeq Davids (SAIAMC, UWC), and Faieq Meyer (SAIAMC, UWC) for their aid in SEM characterization of my samples
- Thank you to Dr. Sivakumar Pasupathi, Dr. Bernard Bladergroen, and Dr. Lindiwe Khotseng for their support for the duration of the research
- Thank you to Dr. Rushanah Mohammed (SAIAMC, UWC) for her training on the Autolab and FRA for Impedance characterization of the samples
- Thank you to the National Research Foundation (NRF) for financial assistance
- A very special thanks to my fellow colleagues who created a friendly and helpful work environment.



## ***Abstract***

Polymer electrolyte membrane (PEM) fuel cells require anode and cathode catalyst layers that are highly efficient and electrochemically active. Platinum electrocatalyst is the most widely used catalyst for PEM fuel cell applications. One of the main drawbacks of this metal is its relative high cost; this has a large contribution to the cost of the entire PEM fuel cell system. The high cost of PEM fuel cell components is one of the main issues hindering the commercialisation of PEM fuel cells.

The main objective of this work is to produce membrane electrode assemblies (MEAs) that have improved performance over MEAs produced by the conventional manner, by producing highly efficient, electroactive, uniform catalyst layers with lower quantities of platinum electrocatalyst. The catalyst coated membrane (CCM) method was used to prepare the MEAs for the PEM fuel cell as it has been reported that this method of MEA fabrication can improve the performance of PEM fuel cells. The MEAs performances were evaluated using polarisation studies on a single cell. A comparison of polarisation curves between CCM MEAs and MEAs produced in the conventional manner illustrated that CCM MEAs have improved performance at high current densities ( $>800 \text{ mA/cm}^2$ ).

The platinum loading (anode and cathode) of the CCM MEAs was varied from  $0.4 \text{ mg/cm}^2$  to  $0.05 \text{ mg/cm}^2$  Pt, with the  $0.4 \text{ mg/cm}^2$  Pt loading MEA achieving current densities of  $4320 \text{ mA/cm}^2$  and power densities of  $1.58 \text{ W/cm}^2$ . The  $0.05 \text{ mg/cm}^2$  MEA reached current densities of  $3920 \text{ mA/cm}^2$  and power densities of  $1.2 \text{ W/cm}^2$ , which is impressive considering the platinum loading was reduced by 87.5 %. This study has shown that the CCM method can enhance platinum utilisation and improve the efficiency of the electrocatalyst.

Operating parameters such as temperature and pressure were investigated to ascertain the influences they have on the performance of the PEM fuel cell. The influence of structural

parameters such as membrane thickness was also investigated on Nafion<sup>®</sup> NRE 212 (50  $\mu\text{m}$  thick) and Nafion<sup>®</sup> NRE 211 (25  $\mu\text{m}$  thick). Peak performance was obtained at operating temperatures of 70 °C and pressures of 2 bar using Nafion<sup>®</sup> NRE 211 membranes.

Nafion<sup>®</sup> content in the catalyst layer was investigated using electrochemical impedance spectroscopy (EIS) and the optimum Nafion<sup>®</sup> amount was found to be 15 wt.%. Scanning electron microscopy (SEM) revealed uniform catalyst layers and close contact between electrolyte and catalyst layers. These results confirm the EIS analysis which show that cell resistances can be decreased by optimising structural and operational parameters of the fuel cell.



## List of figures

<b>Figure 1.1:</b> Schematic diagram of a PEM fuel cell.....	3
<b>Figure 2.1:</b> Chemical structure of Nafion <sup>®</sup> membrane .....	24
<b>Figure 2.2:</b> HydroGen3, fuel cell car .....	27
<b>Figure 2.3:</b> Proton transport model for Nafion <sup>®</sup> membranes .....	30
<b>Figure 3.1:</b> Photograph of a CCM.....	40
<b>Figure 4.1:</b> Comparison of GDL-based MEAs to CCM MEAs.....	44
<b>Figure 4.2:</b> Polarisation and power density curves for PEMFCs with different membrane thickness.....	46
<b>Figure 4.3:</b> Polarisation curves for NRE 211 CCM MEA illustrating the effect of pressure on cell performance.....	47
<b>Figure 4.4:</b> Power density curves for NRE 211 CCM MEA illustrating the effect of pressure on cell performance.....	48
<b>Figure 4.5:</b> <i>In situ</i> impedance curves of NRE 211 CCM MEA at different pressures...49	49
<b>Figure 4.6:</b> Effect of temperature on performance of NRE 211 CCM MEA.....	50
<b>Figure 4.7:</b> <i>In situ</i> impedance curves of NRE 211 CCM MEA at different temperatures.....	51
<b>Figure 4.8:</b> Effect of platinum loading on performance of NRE 211 CCM MEAs prepared with several Pt contents .....	53
<b>Figure 4.9:</b> <i>In situ</i> impedance curves of NRE 211 CCM MEAs with various Pt loadings.....	54
<b>Figure 4.10:</b> Effect of cathode platinum loading on performance of NRE 211 CCM MEAs (70 °C, 2 bar).....	56
<b>Figure 4.11:</b> <i>In situ</i> curves for NRE 211 CCM MEAs having different cathode platinum loadings.....	57
<b>Figure 4.12:</b> <i>In situ</i> impedance curves of NRE 211 CCM MEAs with various Nafion <sup>®</sup> content.....	58
<b>Figure 4.13:</b> <i>In situ</i> impedance curves of NRE 211 CCM MEA at various cell voltages.....	60
<b>Figure 4.14:</b> SEM images of a cross-section of a CCM MEA at 200 x magnification .....	61

**Figure 4.15:** SEM image of a cross-section of a CCM MEA at 600 x magnification.....62

**Figure 4.16:** SEM image of a cross-section of a CCM MEA at 1000 x magnification.....62

**List of tables**

**Table 2.1:** Fuel cell types and features.....9

**Table 3.1:** Chemicals and materials used for preparation of CCMs.....38

**Table 3.2:** Chemicals and materials used for preparation of GDL.....38

**Table 4.1:** Resistances of NRE 211 CCM MEA at different pressures.....48

**Table 4.2:** Resistances of NRE 211 CCM MEA at different temperatures.....51

**Table 4.3:** Cell resistances of various Pt loading NRE 211 CCM MEAs, at different temperatures and pressures.....55

**Table 4.4:** Resistances of NRE 211 CCM MEAs, cathode platinum loading effect.....57

**Table 4.5:** Resistances of single cells with various NRE 211 CCM MEAs.....59

**Table 4.6:** Resistances of NRE 211 CCM MEA at different cell voltages.....61



**List of abbreviations**

<b>AFC</b>	Alkaline fuel cell
<b>AFE</b>	Antiflooding electrode
<b>APU</b>	Auxiliary power units
<b>BEV</b>	Battery hybrid vehicles
<b>CHP</b>	Combined heat and power
<b>CCM</b>	Catalyst coated membrane
<b>DM</b>	Diffusion media
<b>DMFC</b>	Direct methanol fuel cell
<b>DMS</b>	Dimethyl silicon oil

<b>ECA</b>	Electrochemical active area
<b>EIS</b>	Electrochemical impedance spectroscopy
<b>ERP</b>	Electrolyte reservoir plate
<b>GDE</b>	Gas diffusion electrode
<b>GDL</b>	Gas diffusion layer
<b>ICE</b>	Internal combustion engine
<b>MCFC</b>	Molten carbonate fuel cell
<b>MEA</b>	Membrane electrode assembly
<b>PAFC</b>	Phosphoric acid fuel cell
<b>PEM</b>	Polymer electrolyte membrane
<b>PEMFC</b>	Polymer electrolyte membrane fuel cell
<b>PFSA</b>	Perfluorosulfonic acid
<b>PHEV</b>	Plug-in hybrid vehicles
<b>ppm</b>	Parts per million
<b>PSEPVE</b>	Perfluoro sulfonyl fluoride ethyl-propyl-vinyl ether
<b>PTFE</b>	Polytetrafluoroethylene
<b>SEM</b>	Scanning electron microscopy
<b>SOFC</b>	Solid oxide fuel cell
<b>UPS</b>	Uninterruptable power supply
<b>ZSY</b>	Zirconia stabilised with yttria

### **List of symbols**

<b><math>R_{ct}</math></b>	Charge transfer resistance (ohm)
<b><math>R_{\Omega}</math></b>	Ohmic resistance (ohm)



## Table of contents

<b><i>Declaration</i></b> .....	<b><i>ii</i></b>
<b><i>Acknowledgements</i></b> .....	<b><i>iii</i></b>
<b><i>Abstract</i></b> .....	<b><i>iv</i></b>
<b><i>List of tables</i></b> .....	<b><i>vii</i></b>
<b><i>List of abbreviations</i></b> .....	<b><i>vii</i></b>
<b><i>List of symbols</i></b> .....	<b><i>viii</i></b>
<b><i>Chapter 1: Introduction</i></b> .....	<b><i>1</i></b>
1.1 Background.....	1
1.2 Objectives.....	4
1.3 Research structure.....	5
<b><i>Chapter 2: Literature Review</i></b> .....	<b><i>6</i></b>
2.1 Introduction.....	6
2.1.1 Fuel Cells.....	6
2.1.2 Alkaline Fuel Cell (AFC).....	9
2.1.2.1 Introduction.....	9
2.1.2.2 Alkaline Fuel Cell Electrolyte.....	11
2.1.2.3 Alkaline Fuel Cell Electrodes.....	12
2.1.3 Solid Oxide Fuel Cell (SOFC).....	12
2.1.3.1 Introduction.....	12
2.1.3.2 Solid Oxide Fuel Cell Electrolyte.....	14
2.1.3.3 Solid Oxide Fuel Cell Electrodes.....	14
2.1.4 Molten Carbonate Fuel Cell (MCFC).....	15
2.1.4.1 Introduction.....	15
2.1.4.2 Molten Carbonate Fuel Cell Electrolyte.....	16
2.1.4.3 Molten Carbonate Fuel Cell Electrodes.....	17
2.1.5 Phosphoric Acid Fuel Cell (PAFC).....	18

2.1.5.1 Introduction.....	18
2.1.5.2 Phosphoric Acid Fuel Cell Electrolyte.....	19
2.1.5.3 Phosphoric Acid Fuel Cell Electrodes.....	20
2.1.6 Direct Methanol Fuel Cell (DMFC).....	21
2.1.6.1 Introduction.....	21
2.1.6.2 Direct Methanol Fuel Cell Electrolyte.....	21
2.1.6.3 Direct Methanol Fuel Cell Electrodes.....	22
2.1.7 Polymer Electrolyte Membrane Fuel Cell (PEMFC).....	23
2.1.7.1 Introduction.....	23
2.1.7.2 Polymer Electrolyte Membrane Fuel Cell Electrolyte.....	23
2.1.7.3 Polymer Electrolyte Membrane Fuel Cell Electrodes.....	24
2.2 Fuel Cell Applications.....	25
2.2.1 Portable Applications.....	25
2.2.2 Stationary Applications.....	25
2.2.3 Automotive Applications.....	26
2.3 Polymer electrolyte fuel cell components.....	27
2.3.1 Introduction.....	27
2.3.2 PEMFC Structure and Reactions.....	28
2.3.2.1 PEMFC Reactions and Stack components.....	28
2.3.2.2 The Electrolyte membrane.....	29
2.3.2.3 The Electrodes.....	31
2.3.2.4 Gas Diffusion layer.....	31
2.3.2.5 Bipolar plates.....	32
2.4 PEMFC Performance.....	33
2.4.1 Operating Temperature.....	33
2.4.2 Operating Pressure.....	34
2.4.3 Water management.....	35
2.4.4 Membrane Electrode Assembly Parameters.....	36

<b>Chapter 3: Experimental.....</b>	<b>38</b>
3.1 Chemicals and Materials.....	38
3.2 Catalyst layer preparation.....	39
3.3 Gas diffusion layer preparation.....	40
3.4 Fabrication of MEAs.....	40
3.5 Electrochemical Characterisation of MEAs.....	41
3.5.1 Evaluation of MEAs in a single cell.....	41
3.5.2 Electrochemical Impedance Spectroscopy.....	42
3.6 Physiochemical evaluation of MEAs.....	43
3.6.1 Scanning Electron Microscopy.....	43
<b>Chapter 4: Results and Discussion.....</b>	<b>44</b>
4.1 Electrochemical analysis.....	44
4.1.1 Comparing the polarisation curves of CCM and GDL based MEA.....	44
4.1.2 Effect of membrane thickness on cell performance.....	45
4.1.3 Effect of operating pressure on cell performance.....	46
4.1.4 Effect of operating temperature on cell performance.....	50
4.1.5 Performance of MEAs with different platinum loadings.....	52
4.1.6 Effect of cathode platinum loading on cell performance.....	55
4.1.7 Effect on Nafion <sup>®</sup> content in the catalyst layer.....	58
4.1.8 The influence of cell voltage.....	60
4.2 The morphology of CCM MEA.....	61
<b>Chapter 5: Conclusion and recommendations.....</b>	<b>63</b>
5.1 Conclusion.....	63
5.2 Recommendations.....	64
<b>References.....</b>	<b>66</b>

## Chapter 1: Introduction

### 1.1 Background

Global energy and transport systems are based mainly on fossil fuel energy carriers, this dependence on fossil fuels cannot be evaluated as sustainable. Since the world's population is ever growing, there is an ever increasing demand for energy, along with the progressive industrialisation of developing countries. The increasing demand for energy has also led to an increase in greenhouse gas emissions from these fossil fuel-based energy sources, this impacts negatively on our climate system.

Oil is at present the largest primary fuel with a third of the share in the global primary energy mix and more than 95 % of the transport energy demand. Any oil supply disruptions whether due to rising geopolitical tensions, or difficulties in extracting oil from the 'hard to reach' oil reserves the earth has left over, therefore has the hardest impact on the transport sector, since globally, the transport sector is almost entirely dependent on oil. Globally, this has led to mounting anxiety as possible shortages in oil supply and the need to reduce greenhouse gas emissions has led to the search for alternate energy sources [1, 2].

Some of the options being researched include unconventional oil from oil sands or oil shale, synthetic liquids fuels (Fischer-Tropsch Fuels) on the basis of gas or coal, biofuels, electricity as a fuel for battery electric vehicles (BEV) or plug-in hybrid vehicles (PHEV), and hydrogen.

Hydrogen is a secondary energy carrier whose energetic potential lies in its ability to serve as an energy source and medium, convenient for efficient energy storage, transport, as well as being emission-free at the point of final use and thus avoids the transport-induced emissions of both CO<sub>2</sub> and air pollutants [1, 3]. The use of hydrogen as a fuel is based on its oxidation with oxygen, this occurs under normal conditions with strong heat release ( $120.6 \text{ MJ/kg H}_2 =$

33.5 kW h/kg H<sub>2</sub> = 3 kW h/m<sup>3</sup> H<sub>2</sub>). Combustion of 1 m<sup>3</sup> of hydrogen in a power installation with an efficiency of 15-20 % yields 0.45-0.6 kW h, whereas a fuel cell with an efficiency of 40-60 % yields 1.2-1.8 kW h [4].

Fuel cells have the potential to reduce the consumption of fossil fuels through increased energy conversion efficiency. Fuel cells are electrochemical devices that generate electricity from fuel and an oxidant in the presence of an electrolyte. Along with generating electricity it also produces heat and water as a by-product. They offer a wide range of electrical efficiency (ranging from 35-60%) and low emissions, are capable of low temperature operation, provide high quality power, have few moving parts and they provide a continuous source of electrical power without having to recharge.

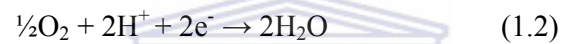
Polymer electrolyte membrane fuel cells (PEMFCs) are considered to be the most suitable replacement for the internal combustion engines (ICEs) used in most transport applications. PEMFCs operate by using hydrogen gas as the fuel source and oxygen/air as the oxidant, they are capable of operating at low temperatures and high current densities, and are considered as one of the most promising technologies capable of producing environmentally friendly energy for portable applications. A PEMFC consists of an external load, two bipolar plates and a membrane electrode assembly (MEA).

The MEA forms the most important part of the fuel cell and consist of a polymer electrolyte membrane sandwiched between the anode and cathode. Figure 1.1 shows a schematic diagram of a hydrogen fuel cell. The most common electrolyte membrane used for PEMFC applications is DuPont's Nafion<sup>®</sup> based membranes which were first developed in the 1960's for the chlor-alkali industry. Nafion<sup>®</sup> is a perflourinated sulphonic acid membrane capable of providing sufficient separation of the H<sub>2</sub> and O<sub>2</sub> gases, while allowing for proton migration through the membrane. Nafion<sup>®</sup> is stable at temperatures of up to 80 °C in PEMFCs, above this temperature the Nafion<sup>®</sup> membrane becomes dehydrated and as a result

loses its conductivity [109]. At the anode of the MEA hydrogen gas is split into protons and electrons according to the following reaction:



The protons are transported through the membrane to the cathode, while the electrons travel through an external circuit thus generating the current output of the cell [2]. At the cathode of the MEA, oxygen molecules react with protons passing through the membrane and electrons from the external circuit to generate water according to the following reaction:



The overall fuel cell reaction taking place is:

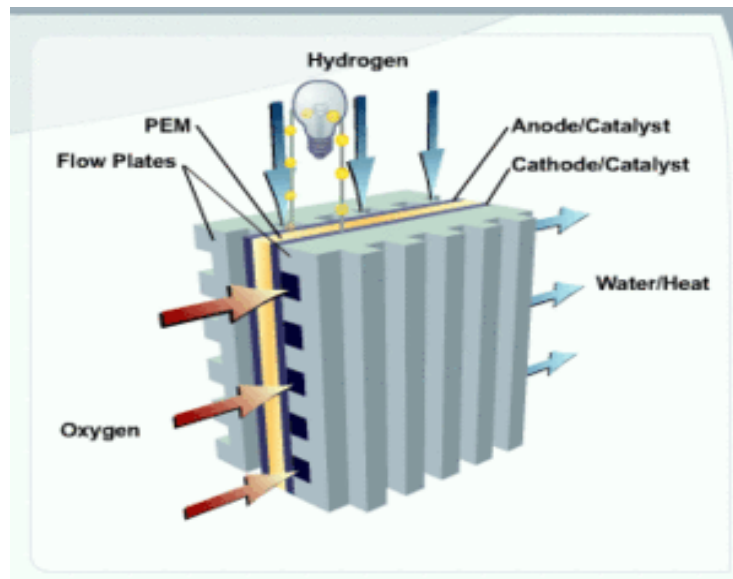


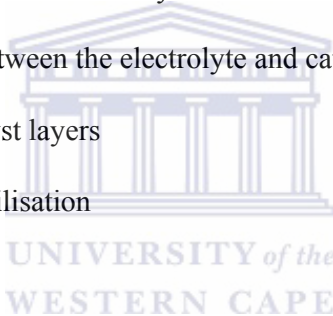
Figure 1.1 Schematic diagram of a PEM fuel cell [5]

PEMFCs are inherently more attractive than ICEs because the electrochemical utilisation of chemical fuels, in this case hydrogen, is more efficient than combustion [2]. This technology is not without its challenges; the relative high cost of PEMFC components is one of the main issues preventing commercialisation.

## ***1.2 Objectives***

The main objective of this study is to develop catalyst coated membrane (CCM) MEAs that have improved performance over the conventional method of MEA fabrication. MEAs produced in this manner would for the following reasons:

- Require lower quantities of platinum catalyst
- Provide improved contact between the electrolyte and catalyst layers
- Produce more uniform catalyst layers
- Provide increased catalyst utilisation



The main objectives of the study are the following:

1. The synthesis of CCM MEAs for PEMFC applications.
2. The catalyst loading of the CCM MEAs will be sequentially reduced and the performance of these reduced catalyst loading MEAs will be evaluated.
3. The optimum Nafion<sup>®</sup> ionomer content in the catalyst layer will be identified.
4. The electrochemical properties of the prepared CCM MEAs will be evaluated and compared to MEAs produced by the conventional method.
5. The CCM MEAs morphology will be characterized, using scanning electron microscopy (SEM), and the electrochemical characterisation of the CCM MEAs will be performed by means of polarisation studies in a single cell and electrochemical

impedance spectroscopy (EIS), the information obtained will be used for the further development of efficient CCM MEAs.

### **1.3 Research Structure**

1. Nafion<sup>®</sup> NRE 212 was chosen for the initial CCM MEA preparation, this electrolyte membrane was chosen because it exhibits high membrane conductivity, the performance of the CCM MEAs were evaluated using various operating parameters.
2. After the achievement of the best performance using NRE 212 membrane, work then commenced on Nafion<sup>®</sup> NRE 211, this membrane exhibits even higher membrane conductivity than NRE 212 membranes.
3. The optimum Nafion<sup>®</sup> ionomer content in the catalyst layer was then established by consulting literature and performing impedance analysis on CCM MEA samples prepared with different Nafion<sup>®</sup> ionomer loading. All CCM MEAs were then prepared using this optimum Nafion<sup>®</sup> amount in the catalyst layer.
4. The initial platinum loading of  $0.4 \text{ mg/cm}^2$  (anode and cathode) was then sequentially reduced to the point where a further reduction in platinum loading would result in too a significant performance loss.
5. The cathode platinum loading was then varied and the CCM MEAs evaluated.



## Chapter 2: Literature Review

### 2.1 Introduction

The literature review focuses on a discussion outlining the various types of fuel cells, their history, composition, the electrode processes involved in their operation, applications, as well as the disadvantages and advantages associated with the different fuel cell types. The outline of the various fuel cell types shows us why we focus on PEMFC for transport and portable applications and an in depth discussion on PEMFC structure and reactions as well as factors which affect PEMFC performance follows. We conclude from this discussion that the CCM method of MEA fabrication is the most suitable for PEMFC MEA fabrication as CCM MEAs exhibit improved performance over conventional GDL-based MEAs.

#### 2.1.1 Fuel Cells

Fuel cells are electrochemical devices that convert chemical energy obtained from the reactants directly into electrical energy and heat, without combustion as an intermediate step. This conversion of energy takes place between the anode and cathode. In this regard fuel cells are very similar to batteries, but unlike batteries, fuel cells never need recharging as they have an external fuel source and as long as the fuel and oxidant is supplied the fuel cell will generate electricity. A fuel cell is thus sometimes referred to as an intermediate between a battery and a combustion engine. However, as batteries and fuel cells are not subject to the Carnot cycle limitations, they may operate with much higher efficiencies than combustion engines and related devices [8]. Fuel cells, unlike combustion engines are not limited by the Carnot efficiency (equation 2.1), but they do have a theoretical limit to their efficiency.

$$\text{Maximum Carnot Efficiency} = \frac{(T_1 - T_2)}{T_1} \quad (2.1)$$

where;  $T_1$  = temperature of heat source;

$T_2$  = temperature of discarded heat.

The efficiency of a fuel cell (Equation 2.2) is usually expressed as the ratio of the electrical output to the heat energy that could be generated by burning the fuel [9].

$$\epsilon_{fc} = \frac{W_e}{\Delta H} \quad (2.2)$$

The maximum possible work obtained from a fuel cell is given by the Gibb's free energy harnessed by the fuel cell and so by modifying equation 2.2, the maximum possible efficiency of a fuel cell is:

$$\epsilon_{max} = \frac{\Delta G}{\Delta H} = 1 - \frac{T\Delta S}{\Delta H} \quad (2.3)$$

The basic operating principle of fuel cells was first discovered in 1801 by Johann Wilhelm Ritter when he reversed water electrolysis and generated electricity from hydrogen and oxygen. The emergence of the internal combustion engine resulted in fuel cell technology remaining undeveloped until the late 1950s. Fuel cell technology literally took off in the early 1960s when NASA utilized fuel cells in the Apollo and Gemini space programs [10]. The driving force behind the renewed interest in fuel cell technology in recent years can be attributed to the global need to address issues such as; the need for efficient energy systems for transportation, the desire to reduce CO<sub>2</sub> emissions and other negative environmental impacts and the demand for high energy density power sources for portable applications [11].

In a typical fuel cell, the fuel is fed to the anode (negative electrode), and oxygen (or air) is fed to the cathode (positive electrode). At the anode of the fuel cell the fuel is oxidized into protons and electrons, the protons travel through the electrolyte to the cathode to combine with oxygen molecules to form water. The electrolyte allows ions to migrate through it and acts as a barrier to gas diffusion. The electrons produced at the anode are carried through an external circuit where they can be made to do useful work, such as powering an electrical motor [9]. Besides the direct production of electricity, heat is also produced in fuel cells. This heat can be used in combined heat and power (CHP) systems, or, in some high temperature fuel cells, for the production of further electrical energy using turbines [12].

Fuel cells are generally classified according to the type of electrolyte material the cell contains. Electrolytes which conduct protons, hydroxide ions, oxide ions, hydronium ions and carbonate ions etc. are used in fuel cells. Ion conduction is a thermally activated process and as a result its magnitude differs from one electrolyte to the next. The type of electrolyte, which may be either a liquid or solid, determines the temperature at which the fuel cell is operated [13]. (See Table 2.1)

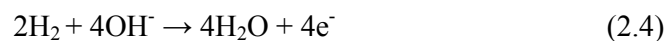
**Table 2.1:** Fuel cell types and features

Fuel Cell Type	Fuel	Electrolyte	Mobile ion	Electrical Efficiency	Operating Temperature
<b>Polymer electrolyte membrane (PEM)</b>	H <sub>2</sub>	Solid polymer membrane (Nafion)	(H <sub>2</sub> O) <sub>n</sub> H <sup>+</sup>	~58%	<100 °C
<b>Alkaline (AFC)</b>	H <sub>2</sub>	Aqueous H <sub>2</sub>	OH <sup>-</sup>	~60%	150-200 °C
<b>Phosphoric acid (PAFC)</b>	H <sub>2</sub>	H <sub>3</sub> PO <sub>4</sub>	H <sup>+</sup>	>40%	150-200 °C
<b>Molten carbonate (MCFC)</b>	Hydrocarbons, CO	(Na,K) <sub>2</sub> CO <sub>3</sub>	CO <sub>3</sub> <sup>2-</sup>	45-47%	600-700 °C
<b>Solid oxide (SOFC)</b>	Hydrocarbons, CO	(Zr,Y)O <sub>2-δ</sub>	O <sup>2-</sup>	35-43%	700-1000 °C
<b>Direct Methanol (DMFC)</b>	CH <sub>3</sub> OH	Solid polymer membrane (Nafion)	H <sup>+</sup>	35-40%	<100 °C

## 2.1.2 Alkaline Fuel Cell (AFC)

### 2.1.2.1 Introduction

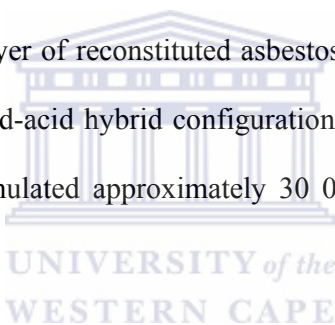
The alkaline fuel cell (AFC) was first developed in the 1930s by F.T. Bacon, and along with J.S. Frost he demonstrated the feasibility of the first fuel generator of 6 kW at Cambridge in 1956 [10]. Their electrolyte consists of potassium hydroxide at different concentrations and different temperatures, while the fuel is pure hydrogen. Hydrogen is oxidised to water at the anode according to the following reaction:



The electrons pass round an external circuit to the cathode, where oxygen is reduced and forms new  $\text{OH}^-$  ions (equation 2.5).



They provided the electrical power and portable water, and were the first fuel cells to be used in the Gemini and Apollo space program and are still used today in the Space Shuttle program [9]. The Space Shuttle cells differ from the Apollo cell in the electrolyte supply structure, which is now based on immobilised 34-46% potassium hydroxide (KOH) electrolyte absorbed in a thin layer of reconstituted asbestos separator. Kordesch equipped a passenger car with an AFC/lead-acid hybrid configuration in the early 1970s. This vehicle operated for 3 years and accumulated approximately 30 000 km during its actual 1000 h operation of the fuel cell [14].



AFCs have the advantage of noticeably lower cathode overpotentials than that found with the acid (including PEM) fuel cells. The more facile hydrogen and oxygen kinetics in alkaline fuel cells results in higher cell voltages. The higher voltage is not solely caused by the improved kinetics, but can also be attributed to the fact that the oxygen reaction via the intermediate peroxide ( $\text{HO}_2^-$ ) in alkaline electrolytes is more facile. This permits the use of non-noble metal catalysts, such as Raney nickel, for the fuel electrode. Silver and spinel-type oxides along with iron phthalocyanines and other porphyrins are good catalysts for the cathodes. These catalysts cannot be used in acidic electrolytes, as they are soluble in acidic media. The AFC operates at up to  $1 \text{ A/cm}^2$  at  $0.7 \text{ V}$  [8].

AFCs main disadvantage relates to terrestrial applications using air or hydrogen derived from hydrocarbons, both of which will contain CO<sub>2</sub>. The alkaline electrolyte, usually potassium hydroxide, reacts with the CO<sub>2</sub> to form potassium carbonate. The main consequences of which are:

- The reduction in OH<sup>-</sup> concentration reduces the rate of the reaction at the anode.
- The carbonate is less soluble, so will eventually precipitate out, blocking the pores of the electrodes.
- Oxygen solubility is reduced increasing the activation losses at the cathode.
- The electrolyte conductivity is reduced, increasing the ohmic losses

These problems can only be overcome by the extensive filtering of the gases to remove the CO<sub>2</sub>. This however, adds to the complexity of the system, cost, size and weight, and complicates servicing. The fact that water is produced at the anode is a further complication, as it means the fuel gas must be circulated actively, with the product water condensed out [9].

### ***2.1.2.2 Alkaline fuel cell electrolyte***

The KOH solution used as the electrolyte can be utilised in liquid form (mobile) or it can be retained in a matrix (static). The advantage of the static system is that the electrolyte is for all intents and purposes solid, and can be in any orientation. This arrangement is used in the Apollo and shuttle fuel cell systems. However, for terrestrial applications the mobile system is used, as it permits reasonably easy renewal of the electrolyte [41]. The circulation of the electrolyte assists in keeping the cell cool, but it adds to the complexity and costs of the system, as the corrosive electrolyte is not easy to handle.

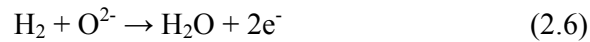
### ***2.1.2.3 Alkaline fuel cell electrodes***

AFCs using nickel electrodes are easily achievable, and many notable cells, including the Bacon cell and Apollo systems, use nickel as the anode catalyst, and nickel oxide as the cathode catalyst. However, the penalty for these easily made electrodes was that the cell had to operate at high pressure, or temperature, or both. This is illustrated by the Apollo systems which operated at pressure of 3.4 bar and a temperature of 230 °C. Platinum metal catalysts are often used in lower temperature systems, and these tend to be rolled onto a nickel mesh support and bound with polytetrafluoroethylene (PTFE), which because of its hydrophobic properties, expels the product water. A thin PTFE layer on the gas side prevents the egress of KOH solution, but allows for the entry of reactant gases.

### ***2.1.3 Solid Oxide Fuel Cell (SOFC)***

#### ***2.1.3.1 Introduction***

The solid oxide fuel cell (SOFC) was developed in 1937 by Baur and Preis out of a need for a more manageable electrolyte as an alternative to the liquid electrolyte. It uses an oxide ion-conducting ceramic as the electrolyte and as the SOFC is a completely solid-state device it is simpler in concept than the other fuel cells as only two phases (gas and solid) are required. The high temperature at which SOFCs operate means that precious metal catalysts are not required and they do not have the electrolyte management issues that occur with phosphoric acid fuel cells (PAFCs) and molten carbonate fuel cells (MCFCs). Both hydrogen and carbon monoxide (CO) can act as the fuel in SOFCs. In SOFCs the negatively charged ion ( $O^{2-}$ ) is transferred from the cathode to the anode through the electrolyte, with the formation of product water at the anode. (See equation 2.6)



The majority of SOFCs are based on an electrolyte of zirconia stabilised with the addition of a small percentage of yttria ( $\text{Y}_2\text{O}_3$ ). At temperatures above  $\sim 700$  °C stabilised zirconia possess an adequate level of oxygen ion ( $\text{O}^{2-}$ ) conductivity, and as a result the SOFC typically operates between  $\sim 700$  and  $1100$  °C. This is the highest operating temperature of all fuel cells, which presents challenges for both construction and durability [9].

SOFCs do not suffer from poisoning, leakage, or evaporation problems experienced by the other fuel cell types and have shown tremendous reliability when operated continuously. For example, a 100 kW system fabricated by Siemens-Westinghouse has successfully produced power for over 20 000 h without any measurable degradation in performance [15]. Such fuel cells offer good fuel flexibility, allowing a variety of hydrocarbon fuels to be utilised.

SOFCs are however still much too costly to for widespread commercialisation, they function poorly under intermittent operation and the possibilities for direct utilisation of hydrocarbon fuels has hardly been explored. The main manufacturing problems are a consequence of the high temperatures required for operation. These problems include brittleness, thermal expansion, and corrosion of the interconnects [13, 18]. The high operating temperatures preclude the use of metals, which typically have lower fabrication costs than ceramics, for any of the non-electrochemical components of the fuel cell and also increase the chances of cracks developing under thermal cycling. While SOFCs offer good fuel flexibility, allowing a variety of hydrocarbon fuels to be utilised, the less reactive fuels must typically be internally steam reformed, that is, reacted with  $\text{H}_2\text{O}$  in the anode chamber, to produce and  $\text{H}_2$  which can subsequently be utilised in the electrochemical reactions [16]. Although not



anticipated to prevent SOFC commercialisation, internal steam reforming requires recirculation of water, and its elimination simplifies fuel cell operation and reduces costs.

Research is currently focused on finding alternative materials to operate with comparable performance at lower temperature. Although operating at lower temperatures appear to be desirable, any measure which significantly reduces the oxide ion mobility would lead to an unacceptably high resistivity and thus poor performance [14].

### ***2.1.3.2 Solid Oxide Fuel Cell Electrolyte***

Zirconia stabilised with yttria (ZSY) is usually the standard electrolyte for high temperature SOFC, although several others have been investigated including  $\text{Bi}_2\text{O}_3$ ,  $\text{CeO}_2$ ,  $\text{Ta}_2\text{O}_5$  and  $\text{LaGaO}_3$ . Zirconia is highly stable in both reducing and oxidising environments and the ionic conductivity of ZSY (0.02 S/cm at 800 °C and 0.1 S/cm at 1000 °C) is comparable with that of liquid electrolytes. The electrolyte layer can be made very thin (25-50 micron) ensuring that the ohmic loss in SOFC is comparable with other fuel cell types. A small quantity of alumina may be added to the ZSY to improve its mechanical stability, and tetragonal phase zirconia has also been added to ZSY to strengthen the electrolyte structure so that thinner materials can be made.

### ***2.1.2.3 Solid Oxide Fuel Cell Electrodes***

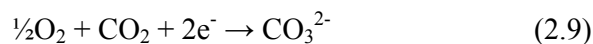
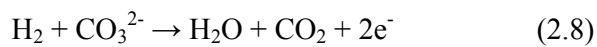
The anode of the state-of-the-art SOFCs is a cermet made of metallic nickel and a yttria stabilised zirconia skeleton. The function of the zirconia is to inhibit sintering of metal particles and to provide a thermal expansion coefficient comparable to that of the electrolyte. The anode and cathode is highly porous so that mass transport of the reactant and product gases is promoted. Strontium doped lanthanum manganite, a p-type semiconductor is the

most commonly used cathode material. Other materials such as p-type conducting perovskite structures, which exhibit mixed ionic and electronic conductivity may also be used [9].

## **2.1.4 Molten Carbonate Fuel Cell (MCFC)**

### **2.1.4.1 Introduction**

In 1960 G.H.J. Broers and J.A.A. Ketelaar reported a high temperature fuel cell that ran for six months, this high temperature fuel cell employed an electrolyte comprised of a mixture of alkali metal carbonates constrained within a disc of magnesium oxide [17]. This was the first MCFC. The alkali metal carbonates in MCFCs are usually a binary mixture of lithium and potassium, or lithium and sodium carbonates, which is retained in LiAlO<sub>2</sub> matrix. At the high operating temperatures of approximately 600-700 °C, the alkali carbonates form a highly conductive molten salt, with the carbonate ion (CO<sub>3</sub><sup>2-</sup>) providing the ion conduction. At the anode of the MCFC hydrogen reduces CO<sub>3</sub><sup>2-</sup> to CO<sub>2</sub> releasing two electrons and generating the electrical power. (See equation 2.8)



On the cathode side, oxygen reacts with carbon dioxide to reform the carbonate ion [18] (see equation 2.9). The need for CO<sub>2</sub> at the cathode (see equation 2.9) requires a scheme that will introduce CO<sub>2</sub> at the cathode, this is usually accomplished by routing the CO<sub>2</sub> generated at the anode (see equation 2.8) to the cathode. The high operating temperature enables the use of non-noble metal catalysts and provides the opportunity to achieve higher overall system

efficiencies with greater flexibility in the use of available fuels. The fuels range from hydrogen to CO containing gases. On the other hand, the higher operating temperature has the disadvantage of placing enormous demands on the corrosion stability and life cycle of the cell components, particularly in the aggressive environment of the molten carbonate electrolyte [19]. The corrosion processes that take place within the cell often cause a permanent loss of electrolyte by forming products containing lithium or potassium. This can cause a total loss of over 20% of the electrolyte during operation. An oxide layer is formed as a result of the corrosion and this can have a high resistance that results in a decrease in cell potential [20].



#### ***2.1.4.2 Molten Carbonate Fuel Cell Electrolyte***

MCFC electrolytes typically contain 60 wt. % carbonate retained in a matrix of 40 wt. %  $\text{LiAlO}_2$ . The  $\gamma$  form of  $\text{LiAlO}_2$  is the most stable in the MCFC electrolyte and is used in the form of fibres of <1-micron diameter. Other materials such as larger particles of  $\text{LiAlO}_2$  may be added. Manufacture of the matrix occurs by using tape-casting methods commonly employed in the ceramics and electronics industry. The ohmic resistance of the MCFC electrolyte, and most importantly the ceramic matrix, has a large effect on the operating voltage, compared with other fuel cells. Under standard MCFC operating conditions the electrolyte accounts for approximately 70% of the ohmic losses. The resistance of the electrolyte can be reduced by making it thinner. There is however a tradeoff between low resistance and long term stability, which is aided by thicker materials [9]. The electrolyte composition affects the performance and endurance of MCFCs in several ways. Li-rich electrolytes have a relatively high ionic conductivity of  $\text{Li}_2\text{CO}_3$  compared to that of  $\text{Na}_2\text{CO}_3$  and  $\text{K}_2\text{CO}_3$ , and as a consequence higher conductivities and hence lower ohmic polarisation

are achieved with Li-rich electrolytes. The gas solubility and diffusivity are however lower, and corrosion is more rapid in  $\text{Li}_2\text{CO}_3$  [19].

#### ***2.1.4.3 Molten Carbonate Fuel Cell Electrodes***

MCFC anodes are usually made of porous sintered Ni-Cr/Ni-Al alloy with a thickness of 0.4-0.8 mm and a porosity of between 55 and 75%, while the cathodes are made of lithiated nickel oxide, with a thickness of 0.5-1 mm. The major problems associated with Ni-based anodes and NiO cathodes are structural stability and NiO dissolution respectively [19]. The anodes are fabricated by hot pressing or by tape casting the powdered material, which is subsequently sintered. Chromium (usually 10–20%) is added to the nickel to reduce the sintering of the anode during cell operation. Sintering and mechanical deformation of the anode under compressive load can lead to growth in pore sizes, loss of surface area, and a decay in MCFC performance by redistribution of carbonate from the electrolyte. The chromium added to the anode is also lithiated by the electrolyte, which then depletes the electrolyte. Aluminium can be added to the anode, which improves both creep resistance in the anode, and electrolyte loss [17]. The cost of Ni-Cr/Ni-Al alloy is relatively high and developers are investigating alternative materials. The partial substitution of the nickel with copper can aid in the reduction of material costs.

Because of the high MCFC operating temperatures, the anode reaction is relatively fast and a high surface area is not required, as is the case with the cathode. Partial flooding of the anode with molten carbonate thus has a good effect in that it can act as a reservoir for carbonate [9].

The cathode material should have sufficient electrical conductivity, structural strength, and low dissolution rate in molten alkali carbonates to avoid precipitation of the metal in the electrolyte structure [19]. The major problem with MCFCs is that the nickel oxide cathode material has a small, but nonetheless significant solubility in molten carbonates. Nickel ions

are formed in the electrolyte through this dissolution and these ions migrate to the anode where they can precipitate out in the electrolyte. Short-circuits of the MCFC and subsequent loss of power are a direct result of the precipitation of the nickel. This problem can be alleviated by using more basic, rather than acidic carbonates in the electrolyte, as well as by operating the fuel cell at atmospheric pressure, keeping a low CO<sub>2</sub> partial pressure in the cathode, and by using a relatively thick electrolyte matrix [9].

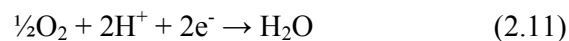
## **2.1.5 Phosphoric Acid Fuel Cell (PAFC)**

### **2.1.5.1 Introduction**

The PAFC was the first fuel cell to be commercialised, it operates at temperatures between 175-200 °C, and uses oxygen as the oxidant and hydrogen as the fuel. The operating temperature is a compromise between the electrolyte conductivity, which increases with temperature, and cell life, which decreases with temperature [21]. PAFCs utilise phosphoric acid as the electrolyte and unlike PEM and AFC, it is reasonably tolerant towards CO impurities contained in the hydrocarbon fuels on which it operates [22]. Hydrogen is reduced at the anode according to the following reaction:



While at the cathode, oxygen is oxidised according to equation 2.11



Platinum electrocatalysts incorporated into porous hydrophobic carbon electrodes are utilised in PAFC systems, and increase costs for these systems. The highly corrosive phosphoric acid electrolyte requires the use of expensive materials, such as teflon and graphite separators [14].

### ***2.1.5.2 Phosphoric Acid Fuel Cell Electrolyte***

Phosphoric acid has good thermal, chemical, and electrochemical stability and therefore makes for a good choice as an electrolyte [21]. In the first stage of PAFC development, phosphoric acid ( $\text{H}_3\text{PO}_4$ ) was diluted to avoid material corrosion, while 100%  $\text{H}_3\text{PO}_2$  is currently used [23]. Because of possible liquid loss, caused by vaporisation, it is necessary to refill the electrolyte, or to provide the cell with an excess of electrolyte before it is operated. The current solution is to create an electrolyte reservoir plate (ERP), made of porous graphite, that provides sufficient electrolyte to operate the cell for 40 000 h [19].

One of the most important components of the PAFC with regards to cell performance and lifetime is the electrolyte-retaining matrix [24].  $\text{H}_3\text{PO}_4$  is retained in a 0.1-0.2 mm thick silica carbide (SiC) matrix. The ohmic resistance of the SiC matrix is very low, due to its thinness, while the mechanical properties are somewhat limited. In fact, the pressure difference between the anode and cathode cannot exceed 200 mbar [23]. The morphology of the matrix is dependent on the properties of the slurry. PTFE, if often added to the SiC to act as a binder. In order to achieve a good performance in the cell, the electrolyte matrix has to be wettable to a certain degree to provide good ionic conduction. Particle size distribution, solid loading, and the electrostatic interaction between the particles in the slurry are some of the physical parameters which control the properties of the matrix layer [25, 26].

### ***2.1.5.3 Phosphoric Acid Fuel Cell Electrodes***

PAFCs use gas diffusion electrodes (GDEs), and since the electrolyte is in liquid form, the electrodes have to be hydrophobic to expel product water. This is achieved by immersing the backing layer into a PTFE solution. PTFE is used as a binder to prevent flooding of the electrodes pores. In the 1960s, both the anode and the cathode were made of PTFE-bound Pt black and the Pt load was  $9 \text{ mg/cm}^2$ . Since then, Pt supported on carbon (Pt/C) has replaced Pt black as the electrocatalyst, and this has allowed for a significant reduction in Pt loading. The carbon is bonded with PTFE and serves three main functions, namely;

- To disperse the Pt to ensure good catalyst utilisation
- To provide micropores in the electrodes to allow for maximum gas diffusion to the catalyst and electrode-electrolyte interface
- To increase the electrical conductivity of the catalyst [9]

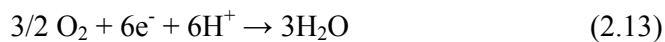
UNIVERSITY of the  
WESTERN CAPE

The use of carbon comes with its own set of obstacles, namely the corrosion of carbon which takes place at high cell voltages. PAFCs should be operated at potentials of less than 0.8 V, otherwise there is a possibility of corrosion occurring, Passalacqua et al. [27] investigated the influence Pt content had on the corrosion phenomena. Their results showed that at high potentials anodic dissolution occurred, therefore no metal is available to catalyse the corrosion of carbon. Platinum also has the tendency to migrate to the surface of the carbon, where it agglomerates in large areas and hence reduces the active surface area [21, 23].

## **2.1.6 Direct Methanol Fuel Cell**

### **2.1.6.1 Introduction**

Direct methanol fuel cells (DMFCs) utilise methanol as a source of energy, and consists of an anode at which methanol is oxidised (see Equation 2.12) and a cathode at which oxygen is reduced to water or steam [28] (see equation 2.13).



Two types of DMFC exist; passive and active DMFCs. Passive-feed DMFCs operate without the assistance of external devices for the pumping of methanol and blowing air into the cell. Oxygen hence diffuses into the cathode from ambient air, and methanol diffuses into the anode from a built-in-fuel reservoir driven by a concentration gradient between the anode and the reservoir [29]. Passive DMFCs hence have much simpler structure and more compact design than active DMFCs, and have the advantages of significant reductions in parasitic power loss and system volume. Some active-feed DMFCs make use of a pump to create circulation of the water product to dilute the methanol reactant, resulting in a more efficient system. Active systems are more reliable and achieve higher performance than passive-feed DMFCs [30].

### **2.1.6.2 Direct Methanol Fuel Cell Electrolyte**

Nafion<sup>®</sup> from DuPont is the most commonly used electrolyte membrane in DMFCs. The Nafion<sup>®</sup> electrolyte is relatively durable (with an unsurpassed longevity of greater than 60 000 h in the PEMFC), and has high ionic conductivity and chemical stability. However, Nafion<sup>®</sup> membranes are not without disadvantages for DMFC applications, including high

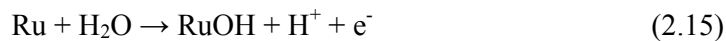
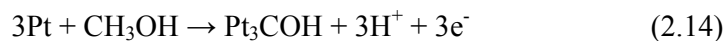


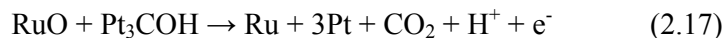
methanol and ruthenium (for Pt-Ru anodes) crossover, high cost, low temperature limit (<80 °C) and high humidification, which are the major barriers preventing Nafion® membranes from being used successfully in DMFCs [30].

Methanol crossover results not only in decreased fuel utilisation, but also a decrease in the overall cell voltage due to the mixed potential on the cathode. Methanol crossover occurs when methanol molecules diffuse from the anode, through the membrane, to the cathode where the molecules are directly oxidised by oxygen. It occurs in part because of molecular diffusion and in part because of the electro-osmotic drag. It has been shown that molecular diffusion mechanism dominates under open circuit conditions and low current densities, whereas the electro-osmotic drag mechanism is more important at high current densities [31, 32].

### ***2.1.6.3 Direct Methanol Fuel Cell Electrodes***

The major problem associated with DMFCs is that the oxidation of methanol (see equation 2.12) does not proceed as readily as for hydrogen. A direct consequence being that there is a considerable overvoltage at the fuel anode. A particularly important problem is the intermediate products of the reaction, which can include CO [9]. Porous carbon electrodes coated with Pt/C are used for the cathode, while Pt-Ru coated on carbon electrodes are used for the anode. Studies have shown that ruthenium increases the catalytic activity of platinum with the optimum composition being 50% Pt and 50% Ru [33]. Methanol oxidation on Pt-Ru particles proceeds through the following steps:





Pt-Ru alloys are used at the anode due to the ability of Ru to electrooxidise CO adsorbed onto Pt. [8]

## ***2.1.7 Polymer Electrolyte Membrane Fuel Cell (PEMFC)***

### ***2.1.7.1 Introduction***

Polymer electrolyte membrane fuel cells (PEMFCs) are so named after the polymer membrane it uses as the electrolyte. The first PEMFC for commercialization was developed in the 1960s by Willard Thomas Grubb and Lee Niedrach of General Electric. The PEMFC provided an auxiliary power source for NASA's Gemini Space missions [34]. Nafion<sup>®</sup> from DuPont is the most commonly used electrolyte membrane. Adequate membrane hydration is essential for protonic conductivity and this limits the operating temperature of PEMFC to below 100 °C. Because of this low operating temperature, a catalyst, usually platinum is needed to promote the chemical reaction. At these temperatures the precious metal catalysts are susceptible to CO, which poisons the anode. Similar to PAFCs, hydrogen is oxidised at the anode and oxygen is reduced at the cathode according to equation 2.10 and 2.11 respectively [13].

### ***2.1.7.2 Polymer Electrolyte Membrane Fuel Cell Electrolyte***

The electrolyte membrane is the core component of the PEMFC. In order to achieve high efficiencies, the membrane must have high proton conductivity, zero electronic conductivity, adequate mechanical strength and stability, chemical and electrochemical stability under operating conditions [35]. The Nafion<sup>®</sup> membrane most commonly used in PEMFCs, uses

perfluoro sulfonylfluoride ethyl-propyl-vinyl ether (PSEPVE). Ion conduction takes place via sulfonic acid branches within the polymer structure [9, 19].

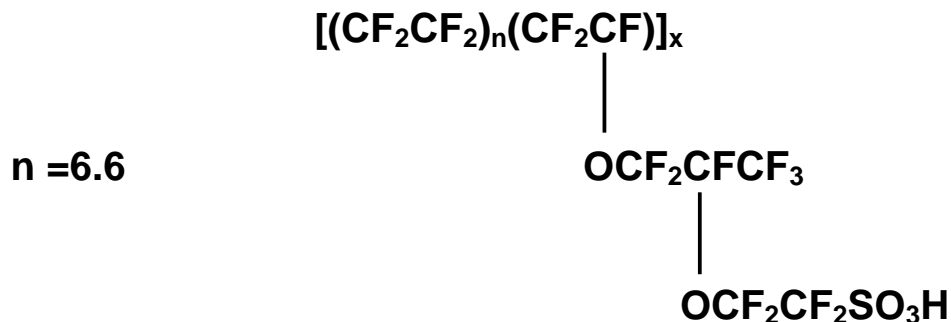


Figure 2.1 Chemical structure of Nafion<sup>®</sup> [7]

Membrane performance is dependent on proton conductivity, which depends on the prevailing levels of hydration. Higher conductivities are, hence supported by higher levels of hydration. For operations with wet membranes, there is however, a possibility of the cathode being flooded, which slows down the oxidation reaction. This is a critical issue with Nafion<sup>®</sup>, because of a phenomenon known as electro-osmotic drag that has been studied by Zawodzinski et al. [36].

### 2.1.7.3 Polymer Electrolyte Membrane Fuel Cell Electrodes

Platinum nano-particles supported on carbon are utilised for both the anode and the cathode. The gas diffusion layer which also serves as the current collector, is typically highly porous carbon paper treated with a hydrophobic polymer [13].

One of the major drawbacks affecting PEMFCs is the high cost of precious metals. Some of the approaches to reduce the Pt metal requirement in PEMFCs include reducing the mass transport losses particularly at high current density by improving the diffusion media (DM),

improving reactant flow fields and improving electrode structures as well as improving the catalysts and catalyst utilisation [37].

## ***2.2 Fuel Cell Applications***

### ***2.2.1 Portable Applications***

Portable fuel cell applications refer to small, grid free, electrical power units ranging from a few watts to one kilowatt. In addition to producing less noise and providing a higher quality of energy production, portable fuel cells also extend the duration of grid independent operation [12]. DMFC technology is primarily used for small portable electronic devices, such as laptop computers and mobile phones, as they have the appropriate characteristic for these applications. They operate at low temperature, do not require electricity to recharge, use a quick refueling system, and can be designed in such a manner as to provide for longer cell lifetime [38-40]. The DMFC has the potential to replace the battery because methanol theoretically has a superior specific energy density in comparison to the best rechargeable batteries currently on the market [30]. PEMFC units, ranging from 50 to 500 W, are also used for applications such as powering microclimate cooling systems.

### ***2.2.2 Stationary Applications***

Fuel cells are developed for stationary power generation applications such as power plants, large and small-scale CHP and micro-CHP. Although fuel cells have the advantage of providing better electrical efficiencies, the efficiency and costs are dependent on the size of the system, i.e. the smaller the system, the more energy and investment is required for the balance of plant equipment in relation to the size of the cells [41]. Conventional uninterruptable power supply (UPS) systems utilise engine generators and/or batteries as their

main sources to provide electric power for critical functions or loads when the normal utility power is not available. Fuel cells, unlike batteries, can provide continuous power for as long as reactants are supplied, this is particularly useful whenever the duration of the power outage is uncertain [42].

PAFCs are currently the most advanced system in terms of commercial development, with several hundred units (~200 kW power), and together with MCFCs they're installed as CHP units in hospitals, government buildings, military bases, commercial premises, and even prisons [9] (see Figure 1.2). In these applications fuel cells can provide high quality, reliable, grid independent, on-site electric power, with reduced emissions compared to conventional power technologies [43].

### ***2.2.3 Automotive Applications***

Fuel cells offer more than double the efficiency of traditional combustion technology. This efficiency results in a more than 50% reduction in fuel consumption when compared to a conventional vehicle that is powered by a gasoline fueled ICE. Fuel cell systems designed for vehicular propulsion must have weight, volume, power density, start-up, and transient response similar to ICE vehicles. PEMFCs are gaining popularity as the fuel cell of choice for vehicular applications because of their low operating temperature. The relatively high problems associated with PEMFC-based technology is that the CO concentration in the fuel should be reduced to less than 10 parts per million (ppm), as a higher CO content in hydrogen contributes to deterioration of the cell performance.

In addition to automotive propulsion, the use of fuel cells as auxiliary power units (APUs) for vehicles offers a true mass-market opportunity that does not require the challenging performance and low cost required for propulsion systems for vehicles. APUs are devices that can provide all or part of the non-propulsion power for vehicles. APUs can be used in a

variety of transportation types including trains, ships, heavy duty and utility trucks, airplanes etcetera. The potential benefits APUs offer include operating when the main engine is unavailable, extending the life of the main engine, reducing emissions and noise while parked, and improving power generation efficiency when parked [19].



**Figure 2.2 HydroGen3, a fuel cell car developed by Adam Opel AG, is propelled by a fuel cell stack consisting of 200 individual PEM fuel cells connected in series [6]**

## ***2.3 Polymer Electrolyte Membrane Fuel Cell Components***

### ***2.3.1 Introduction***

From the discussion leading through the basics of fuel cells, their mode of operation and the type of applications they're used in, we can see that PEMFCs lead the field when it comes to the wide variety of applications they can be utilised in. As discussed previously PEMFC technology is widely recognised as the most suitable for transport applications; in which they would replace the ICE, and portable applications; where they would replace batteries [46]. This technology has several attractive features; they provide high current density, high chemical-to-electrical energy conversion efficiency, and fast and easy start-up.

Low temperature operation allows them to start quickly and easily, and results in less wear and tear on system components. As PEMFCs are the topic of this dissertation, we will now take a more in-depth look at PEMFCs.

## ***2.3.2 PEMFC Structure and Reactions***

### ***2.3.2.1 PEMFC Reactions and Stack Components***

The cathode reaction produces the electrical and heat energy for the cell. The Gibbs energy of the reaction is theoretically available as electrical energy, with the rest of the reaction enthalpy released as heat. In reality, part of the Gibbs energy is converted into heat via the loss mechanisms. The theoretical cell voltage for a hydrogen-oxygen fuel cell at 25 °C is 1.23 V and decreases according to the Nernst equation with decreasing reactant concentration (pressure) and increasing temperature. Because single fuel cells produce a limited voltage, usually less than 1 V, in order for them to produce a useful voltage for practical applications, several unit cells are connected in series to form a fuel cell stack.

The output voltage of the entire stack is determined by the number of unit cells in the stack [47]. PEMFC stacks operating on hydrogen can be up to 40-50% electrically efficient and 80% system efficient (if heat recovery is included) [48]. Fuel cell stacks based on different materials, structures and fabricating techniques have been developed in several countries, with power outputs varying from less than 100 W for portable power applications [49] to that of 1 kW or several kilowatts for use in residential areas [50-54], to 20-75 kW stacks for vehicles [55] and up to 200-250 kW stacks for stationary use.

### ***2.3.2.2 The Electrolyte Membrane***

The polymer electrolyte membrane provides the transport medium for the protons to migrate to the cathode and complete the electric and mass transport circuits. The electrolyte membrane also acts as a barrier, separating hydrogen and oxygen molecules and therefore preventing direct combustion, in addition it also acts as an electronic insulator between the bipolar plates [47]. The membrane therefore needs to possess a high proton conductivity, good durability and minimum fuel crossover. As discussed previously, Nafion<sup>®</sup> membranes are the most commonly used electrolyte membrane in PEMFCs. This perfluorosulfonic acid (PFSA) membrane has hydrophilic side chains terminated with  $-\text{SO}_3\text{H}^+$  groups along the perfluoroethylene backbone. The sulfonic acid molecules are fixed to the polymer backbone and cannot leak out, the protons on these acid groups are, however, free to migrate through the membrane. The ratio between the two co-monomers can vary, hence the bulk capacity of the membrane can also vary. Thickness of the membranes may vary from 50-250  $\mu\text{m}$ , with maximum proton conductivity of such membranes at 30  $^\circ\text{C}$  ranging from 0.2-0.05  $\text{S cm}^{-1}$ , depending on the equivalent weight of the membranes.

Two models for the proton transport in Nafion<sup>®</sup> membranes exist. The Girke's cluster channel model (see Figure 2.3a); in which the membrane polymer matrix is self-organized so that water-filled clusters are formed, with sulfonated side chains turned to them. The clusters are separated by narrow channels which act as a pathway for proton transport. If the water content is low, the channels break, thus preventing proton transport. The other model is a channel model (see Figure 2.3b), according to which membrane transport channels are filled with water, and sulfo groups are separated by hydrophobic polymeric chains. As the water content of the membrane decreases, the channels become narrower, and proton conductivity decreases. The models imply that membranes accomplish proton transport only in the presence of a sufficient amount of absorbed water.



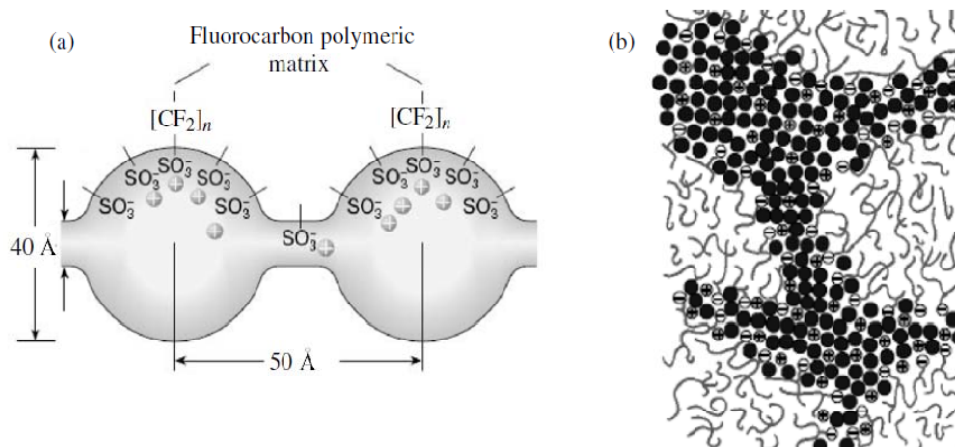


**Figure 2.3 Proton transport models for Nafion® membranes** (a) Cluster-channel and (b) Channel model [53]

Relative humidity has greater impact on conductivity than temperature, although at temperatures above 90 °C conductivity of the membrane drops dramatically due to dehydration if the membrane is not perfectly humidified. The operating temperature of PEMFCs are thus limited to below the boiling point of water and makes water management in PEMFCs very important. The conductivity of the membrane is also sensitive to contamination, for example, if the membrane is exposed to metallic impurities, metal ions diffuse into the membrane and displace the protons as charge carriers, which results in a lower membrane conductivity [47, 56].

Research has also shown that the ionomers performance and intrinsic properties are not only dependent on its chemical identity (ion exchange capacity, anionic functional group, and counter-cation), but also on the method of membrane synthesis (casting or melt-extrusion), the thermal history of the polymer (drying, exposure to high temperature, and membrane pretreatment), and the chemical history of the membrane (exposure to various cations, solvents, etc.) [58].

### ***2.3.2.3 The Electrodes***

The electrochemical reactions all take place on the surface of the electrodes. In order to speed up the cells reactions, the electrodes contain catalyst particles, usually platinum or an alloy of platinum and other noble metals. The low operating temperature and low pH makes the use of catalysts essential [59], especially for the oxygen reduction reaction (ORR) at the cathode, which is extremely slow without the presence of a catalyst. The electrodes are usually made of a porous mixture of carbon supported platinum and ionomer. In order for the electrode reactions to occur, the catalyst needs to be at the boundaries of three phases, i.e. electron conductive phase (carbon), ion conductive phase (Nafion), and gas or liquid phase of reactants and products (pores) [60]. The point where the reactants, catalyst and electrolyte come into contact is conventionally referred to as the triple-phase boundary interface.

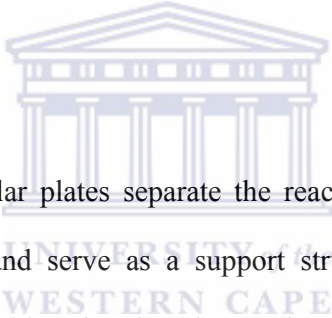
In order to achieve acceptable reaction rates, the effective electrochemical surface area of the active catalyst sites should be several times higher than the geometrical area of the electrode. The electrodes are therefore porous to form a three-dimensional network in which the triple-phase boundaries are located [47]. Most PEMFC developers today have chosen the thin-film approach for their product prototypes, in which the electrodes are manufactured directly on the membrane surface. The benefits of thin-film electrodes include lower cost, better catalyst utilisation and improved mass transport [61]. Thin-film electrode thickness range from 5-15  $\mu\text{m}$ , and the catalyst loading is typically between 0.1-0.3  $\text{mg cm}^{-2}$ . Another option is to manufacture the electrode on the surface of the porous gas diffusion backing, by coating the backing with a mixture of carbon supported catalyst and ionomer.

### ***2.3.2.4 Gas Diffusion Layer***

The gas diffusion layer (GDL) transfers the electrons between the electrodes and bipolar plates, and distributes the reactants from the gas flow channels uniformly along the active

surface of the catalyst layer, which helps the complete utilisation of the electrode area. They are also responsible for the removal of product water from the electrode surface and allow for the transport of water between the electrode and the flow channels. The GDLs are made up of a porous, electrically conductive material, typically carbon cloth or carbon paper. This substrate is usually treated with a fluoropolymer (e.g. PTFE) and carbon black to improve water management and electrical properties respectively [47]. The in-plane and through-plane resistivities of commercial GDLs range from 25-100  $\text{m}\Omega\text{cm}^2$  and 6-20  $\text{m}\Omega\text{cm}^2$  respectively. The in-plane and through-plane resistances are dependent on the microstructure of the GDL. The cell resistance is dictated by the through-plane resistance, whereas the in-plane resistance affects the reaction uniformity [62].

#### **2.3.2.5 Bipolar Plates**



In a fuel cell stack, the bipolar plates separate the reactant gases of the adjacent cells, connect the cells electrically, and serve as a support structure. The bipolar plates have reactant flow channels on both sides, forming the anode and cathode compartments of the unit cells on the opposite sides of the plate. The separator plates in a single cell have flow channels on only one side and sometimes called monopolar plates. The geometry of the flow channels has an effect on reactant flow velocities and mass transfer, and hence also has an effect on the performance of the fuel cell [47].

Bipolar plate materials need to be highly electrically conductive and impermeable to gases. The material should also be resistant to corrosion and chemically inert, due to the presence of reactant gases and catalyst. Most applications also require a low weight and high strength material, with commercial applications requiring a cheap material that is suitable for high-volume manufacturing methods. For PEMFCs, bipolar plates are usually made of resin-impregnated graphite, but stainless steel has also been used [63-65]. Solid graphite has a high

electrical conductivity, is chemically inert and resistant to corrosion, but has the drawback of being expensive and costly to manufacture. Stainless steel on the other hand is cheap, but must often be coated to prevent corrosion and contact resistance, as well as being expensive to machine. The flow channels are machined or electrochemically etched on to the graphite or stainless steel bipolar plate surfaces. However, these methods are not suitable for mass production and therefore new bipolar plate materials are being researched. To date, the best results have been achieved with carbon-polymer composites, which can be molded [66-68].

## ***2.4 PEMFC Performance***

### ***2.4.1 Operating Temperature***

The intrinsic nature of the materials used in PEMFCs enables low temperature operation of approximately 80 °C, and the cell is also able to sustain operation at high current densities. These attributes enable a fast start-up capability and the ability to make a compact and lightweight cell [69]. As a result, PEMFCs are particularly suited for vehicular applications. The low operating temperature is beneficial because it allows the cell to start quickly from ambient conditions, especially when pure hydrogen fuel is used. It has the disadvantage in that platinum catalysts are required to promote the electrochemical reaction. At temperatures below 100 °C CO binds strongly to platinum sites, which in turn reduces the number of sites available for hydrogen chemisorption and electro-oxidation. Due to the effect CO has on the anode, only a few ppm of CO can be tolerated with platinum catalysis at 80 °C.

Cell operating temperature has a significant influence on the performance of PEMFCs, in that an increase in temperature has the effect of lowering the internal resistance of the cell, mainly by decreasing the ohmic resistance of the electrolyte. Mass transport limitations are also reduced at higher temperatures. Hence, as a result an overall improvement in cell

performance is observed. Operating at higher temperatures results in a reduction in the chemisorption of CO, because this reaction is exothermic. Improvement of cell performance through increase in temperature, is however, limited by the high vapour pressure of water in the polymer electrolyte membrane. This is due to the difficulty in maintaining adequate membrane hydration at elevated temperatures, subsequent dehydration of the membrane results in a greater membrane resistance to proton transport and hence loss of ionic conductivity. The performance would be further improved if the membrane could withstand operation at higher temperatures (above 100 °C), but Nafion<sup>®</sup> has a glass transition temperature of approximately 111 °C and hence mechanical stability is compromised at elevated temperatures [62, 70].

#### ***2.4.2 Operating Pressure***

An increase in cell operating pressure has the effect of increasing the overall cell potential. This can be attributed to the reduction in the activation overpotential which occurs with increasing pressure. Higher pressure results in higher concentration of gases through the electrodes due to higher solubility and enhances cell performance. According to the Nernst equation, the increase in the reversible cell cathode potential that is expected for this increase in oxygen pressure is approximately 12 mV, a value which is considerably less than the measured value [70]. A PEMFC operated at 50 °C and 500 mA/cm<sup>2</sup> [71], exhibited a voltage increase of 83 mV for an increase in pressure from 1 to 5 atmospheres. These results indicate that an increase in oxygen pressure resulted in a substantial reduction in the polarization at the cathode. Improvement in the cell performance due to increased pressure must be carefully balanced against the energy required to pressurize the reactant gas [70].

### ***2.4.3 Water management***

Sufficient water content is necessary to maintain the proton conductivity of the membrane, if the membrane water level is insufficient, or the membrane is dry, the resulting decreased proton conductivity will lead to a lower cell performance. A dry membrane is also susceptible to pinhole formation, which can accelerate the degradation process or lead to membrane failure. Excessive liquid water in the cathode or gas diffusion layers, on the other hand limits the reactant mass transport and leads to a drop in performance or cell reversal. Water hence plays an interesting role in PEMFCs; favourable for proton transport and adverse for mass transfer. The preferred method of dealing with water in order to achieve better cell performance is to maintain a balance by providing enough water for proton exchange to occur through the membrane, and avoid condensed liquid water which blocks the mass-transfer channels [71].

Three water transport mechanisms across the membrane exist; (1) electro-osmotic drag in which hydrogen ions carry water molecules with them from the anode to the cathode as they pass through the membrane; (2) back-diffusion by the concentration gradient of water: because the water concentration on the anode differs to the water concentration on the cathode, some water molecules diffuse from the cathode to the anode; (3) convection by means of the pressure gradient: water moves from the higher vapour pressure side to the lower one [72].

Thinner PFSA membranes [73-76] enhance water back diffusion to the anode, which favours water balance at high current densities under conditions of very little or no humidity. M. Ji et al. [77] attempted to solve the problem of water flooding that takes place in the pores of a porous electrode by using an antiflooding electrode (AFE), which contained water-proof oil, dimethyl silicon oil (DMS). Their AFE achieved success due to the fact that oxygen is over ten times more soluble in DMS than it is in water, and hence supplies an unoccupied

channel for oxygen transportation as well as solving flooding in pores with a diameter of 20-70 nm.

#### ***2.4.4 Membrane Electrode Assembly Parameters***

The MEA forms the most important part of the fuel cell, it is made up of the electrolyte membrane sandwiched between the anode and cathode electrodes. One of the main requirements for the commercialisation of fuel cells is the reduction in the cost of the materials used. Because PEMFCs need precious metal electrocatalysts, normally platinum and its alloys, decreasing the amount of catalyst without sacrificing the performance is essential. This can be accomplished by increasing the reaction sites in the catalytic layer, which are in direct contact with membrane and GDL to form the MEA [78]. In addition to the catalyst loading, there are a number of catalyst layer properties that need to be optimised in order to achieve a high catalyst utilisation in the MEA: i.e. reactant diffusivity, ionic and electrical conductivities and the level of hydrophobicity, which have to be carefully balanced [79].

The electrochemical reaction can only occur at the "triple-phase boundaries" within a fuel cell, where the electrolyte, reaction material, and electrically connected catalyst particles come into contact in a MEA. This triple-phase boundary area depends greatly on the method of MEA fabrication as well as structural parameters such as catalyst and ionomer loading [80-84].

At the present time, there are only two modes for fabricating MEAs, in which the electrocatalyst can either be applied onto the gas diffusion layer (GDL-based MEAs), or directly onto an electrolyte membrane (CCM-based MEAs) [85, 86]. Tang et al. [87] performed a comparative investigation on PEM fuel cells with MEAs made in the conventional manner (GDL-based MEAs) and CCM MEAs. Their findings showed that cells

with a CCM MEA exhibit significantly higher performance than those prepared with conventional GDL-based MEAs.

The CCM method improves contact between the catalyst layers and the electrolyte membrane, this can be utilised to effectively reduce the catalyst loading without sacrificing the performance of the cell [88]. There are generally two approaches to reduce the amount of platinum in PEM fuel cells; one method involves the development of an alloyed catalyst based on platinum, which has a better catalytic activity, or to discover a new catalyst [89-91]. The other is to invent a new method for fabricating the catalyst layer, such as pulse electro-deposition, electrospray technique, sputter deposition, pulsed laser deposition and ion-beam deposition [92-95]. With respect to thin film catalyst formation in a fuel cell, supported catalysts and polymer ionomers in the catalyst layer structure has been used to reduce the amount of catalyst from  $4 \text{ mg/cm}^2$  to approximately  $0.4 \text{ mg/cm}^2$ . It has been reported that as the catalyst particle size increases, so the electrochemical active area (ECA) decreases with increased loadings of the supported catalysts. Hence lower loadings of supported catalyst are used because they provide larger electrochemical active areas. [96].

Structural modification affects the mass transport of the reactant gas and water produced during the reaction. The ion and electron transfer is also affected by structure of the catalyst layer, and this in turn affects the overall cell performance [97]. The anode catalyst of the CCM should have a high hydrogen oxidation reaction mass activity in order to produce anode catalyst layers with a minimum of catalyst, that is resistant to CO poisoning and resistant to electrochemical corrosion. Cathode catalysts of the CCM, on the other hand, require high ORR activity, low costs, durability and optimised tortuosity in order to provide adequate rates of proton diffusion via the ionomer network, and reactant gas permeability in the transport pores of the bulk of the cathode catalyst layer [98]. Optimising the MEA hence plays a key role in reducing material costs and is essential for the commercialisation of PEMFC.



## Chapter 3: Experimental

### 3.1 Chemicals and Materials

The chemicals and materials used for the preparation of the CCM and GDL are listed in Table 3.1 and 3.2, respectively.

**Table 3.1:** Chemicals and materials used for preparation of CCMs.

Chemicals and Materials	Supplier
Platinum, nominally 40% on carbon black	Alfa-Aesar
Nafion 5% w/w solution	Alfa-Aesar
Nafion-NRE-212 and 211 membrane	Electrochem, Inc.
Isopropanol	Alfa-Aesar

**Table 3.2:** Chemicals and materials used for preparation of GDL.

Chemicals and Materials	Supplier
Toray Carbon Paper (Teflon treated)	Electrochem, Inc.
Carbon Black (Vulcan XC72)	Cabot
Teflon™ Emulsion Solution TFE 30	Electrochem, Inc.
Isopropanol	Alfa-Aesar

All the water used during the preparation of samples was obtained from a Milli-Q® ultrapure water system. The resistance of the water was 18.3 MΩ.cm.

List of equipment used:

- Muffle furnace with electrical heating (Kiln contracts)
- Ultrasonic bath (Integral Systems)
- Stainless steel heating plate
- Airgun (Prona)

- Vacuum Oven (VM 53 Binder)
- Electronic Load (Arbin Instruments)
- Hot Press (homemade)
- Potentiostat PGSTAT30, Eco Chemie
- Current Booster BSTR10A, Eco Chemie
- Hair dryer (Russel Hobbs, 2000W)

### ***3.2 Catalyst layer preparation***

Commercial 40 wt.% Pt catalyst supported on carbon black (Pt/C) from Alfa-Aesar was used for the cathode and anode in all experiments. To prepare the catalyst ink, a suspension was formed with the desired amounts of Pt/C catalyst (0.05-0.4 mg/cm<sup>2</sup> Pt), Nafion 5% w/w solution (15-35 wt.%), and ultrapure water, having isopropanol as the solvent. The mixture was then dispersed by sonicating in an ultrasonic bath for 2 hours to form an ink before being used.

Nafion<sup>®</sup> NRE 211 and 212 untreated membranes were used as the electrolyte membranes. The membranes were fixed on a stainless steel heating plate, in order to keep the membrane surface flat while spraying, and prevent the formation of wrinkles on the active area of the membrane. The catalyst ink was quantitatively deposited onto both sides of the membrane using an airgun (Prona). The platinum loading was varied from 0.05 to 0.4 mgcm<sup>-2</sup>, the loading was determined by weighing the membrane in the frame before spraying, and then weighing at intervals during the spraying procedure until the desired platinum loading was obtained. The CCM was dried thoroughly before weighing to ensure that all the solvent had evaporated, this was followed by drying in a vacuum oven for 1 h at 80 °C.

### ***3.3 Gas diffusion layer preparation***

To form the gas diffusion layer, a slurry containing carbon black (Vulcan XC72), PTFE 30 wt % emulsion, and ultrapore water, having isopropanol as solvent was formed. This slurry was then dispersed in an ultrasonic bath for 2.5 hours. The carbon paper was sintered in a muffle furnace at 300 °C for 1 h, and the carbon slurry was sprayed onto one side of the paper using an airgun. The carbon paper was weighed at the start, and then at successive intervals until the desired carbon loading of 1 mgcm<sup>-2</sup> without the solvent was obtained. A hair dryer was used to dry the carbon paper during spraying. Final treatment of the GDL involved sintering in the muffle furnace for 1 h at 300 °C.

### ***3.4 Fabrication of MEAs***

The MEAs were prepared by sandwiching the CCM between two GDL electrodes, and hot pressing at 130 °C under a pressure of 15 MPa for 3 min. The active area of the prepared MEAs was 9 cm<sup>2</sup>. Figure 3.1 shows a prepared CCM without the GDL electrodes.

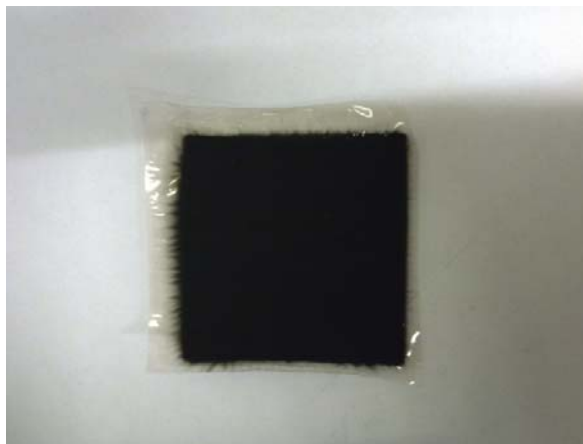


**Figure 3.1. Photograph of a CCM**

### ***3.5 Electrochemical Characterisation of MEAs***

#### ***3.5.1 Evaluation of MEAs in a single cell***

MEAs were placed in a single cell (5 cm<sup>2</sup> active area) with a serpentine flow field. A torque wrench was used to adjust the torque to 4.5 Nm diagonally on each bolt. This was to ensure that equal pressure was applied to the MEA structure inside the cell. Pure oxygen and hydrogen was fed to the cathode and anode, respectively, at flow rates of 2 l/min (oxygen) and 0.5 l/min (hydrogen). Reactant humidification was achieved by bubbling the reactant gases through ultrapure water in stainless steel humidifiers before entry into the cell. The gas connections between the humidifiers and the fuel cell inlets were well insulated to prevent condensation of the water vapour on entry into the fuel cell. The temperature in the humidifiers and fuel cell were controlled by temperature controllers.

An electronic load (Arbin Instruments, USA) connected to a computer was used to evaluate the cells. The MEAs were activated at atmospheric pressure by discharging at 300 mA, at 70 °C for 4 h under 100% relative humidity before measurements were taken. During the activation period, the H<sub>2</sub> gas was fed to the anode at 0.5 l/min, while the O<sub>2</sub> gas was supplied to the cathode at a flow rate of 2 l/min. Performance evaluations were carried out within 30-60 °C cell temperature range. Tests performed at 30°C and 60°C were carried out under atmospheric pressure (atm), while tests performed at 70°C and 80°C were carried out under atmospheric pressure and under back-pressure of 2 bar. Back-pressure was applied to both the anode and cathode by fixing back-pressure regulators at the exhaust of the cell. The temperatures of the humidifier cylinders were varied to alter the water activity of the feed. The humidity of the reactant gases were maintained at 100% relative humidity.

The polarization measurements were recorded by measuring the cell voltage as a function of the current. The measurements were made starting at open circuit voltage (OCV) and increasing the current with each subsequent load condition.

### ***3.5.2 Electrochemical Impedance Spectroscopy***

Electrochemical impedance spectroscopy (EIS) is a technique used to measure the frequency dependence of a fuel cell by applying a small perturbation signal (AC potential or current) to the fuel cell and measuring the current (or potential) response. EIS can be utilised to identify the individual contributions to the total impedance of a PEM fuel cell from different electrode processes such as interfacial charge transfer and mass transport in both the catalyst and backing diffusion layer [95, 96].

The impedance spectra were recorded at various potentials using a potentiostat (Autolab PGSTAT30, Eco Chemie B.V.) equipped with a frequency response analyser (Version 4.9 Eco Chemie B.V.) and a current booster (Autolab BSTR10A, Eco Chemie B.V.). Tests were performed at cell temperatures of 30 °C and 70 °C with 100% relative humidity of reactant gases, and operated at atmospheric pressure. Tests at 70 °C were also performed under back-pressure of 2 bar at both the anode and the cathode. The two-electrode configuration was used; the anode (fed with H<sub>2</sub> gas) was used as the reference and the counter electrode, while the cathode (fed with O<sub>2</sub>) was used as the working electrode. Due to the more facile reaction kinetics of the H<sub>2</sub> oxidation reaction on the Pt/C electrocatalysts as compared to that of the O<sub>2</sub> reduction reaction [97], the cell impedance is mainly dominated by the cathode impedance. The impedance spectra were recorded potentiostatically in the 0.1 Hz to 10 kHz frequency range with a sinusoidal amplitude of 5 mV.

### ***3.6 Physiochemical evaluation of MEAs***

#### ***3.6.1 Scanning Electron Microscopy***

A scanning electron microscope (SEM), Hitachi X-650 SEM using GENESIS software was used to characterise the MEAs structural configuration. SEM was used to observe cross-sections of the MEAs, thickness of the catalyst layers, and the contact between the catalyst layers and the electrolyte membrane of the prepared MEAs.

SEM operating parameters:

Working distance: 15 mm

Accelerating gun filament: Tungsten

Accelerating voltage: 25 KeV

Filament current: 75–80  $\mu$ A



## Chapter 4: Results and discussion

### 4.1 Electrochemical analysis

#### 4.1.1 Comparing the Polarisation curves of CCM and GDL based MEA

The method used to prepare MEAs plays a significant role in the performance of the fuel cell. It is believed that the direct deposition of catalyst onto the electrolyte membrane provides better catalyst utilisation than the GDL-based method. MEAs prepared using the CCM method were compared to previously tested MEAs prepared in the conventional manner (GDL-based) with the exact same ionomer content, catalyst loading, carbon loading and pressing conditions. Figure 4.1 shows the polarization curves illustrating the comparison between a conventional MEA and CCM MEA, both having a platinum loading of  $0.4 \text{ mg/cm}^2$  (anode and cathode).

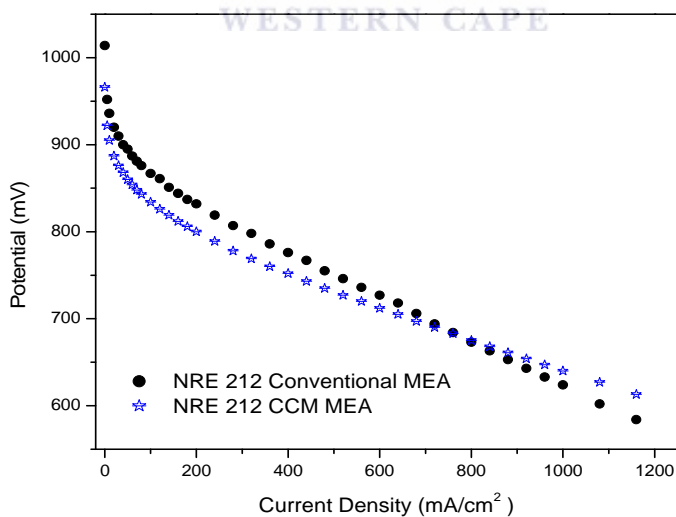


**Fig. 4.1 Comparison of GDL-based MEAs to CCM MEAs  
(70 °C, 2bar)**

The polarization curves illustrate the difference in performance we obtain when utilising different methods of MEA preparation. The MEA prepared in the conventional manner shows improved performance at low and medium current density due to lower ohmic and activation overpotential. However, in the high current density region ( $>800 \text{ mA/cm}^2$ ), the CCM MEA performance increased with increasing current density. A voltage drop at high current density is generally attributed to mass transport limitations occurring in the electrolyte membrane and electrodes. The higher performance of the CCM MEA in the high current density region can thus be explained by less mass transport limitations, likely due to improved interfacial contact between electrolyte and catalyst layers, which would improve transport of reactant gases, especially at high current densities.

#### ***4.1.2 Effect of membrane thickness on cell performance***

The effect of membrane thickness on cell performance can be seen in Figure 4.2; in the low current density region ( $<170 \text{ mA/cm}^2$ ), the cell with the thicker membrane, Nafion<sup>®</sup> NRE 212 (50  $\mu\text{m}$  thick) showed a slightly better performance. This can be attributed to the fact that thicker membranes will have less fuel cross-over, which would lead to a lower mixed potential on the cathode. While in the medium and high current density region ( $>300 \text{ mA/cm}^2$ ), the cell with the thinner membrane, Nafion<sup>®</sup> NRE 211 (25  $\mu\text{m}$  thick), gave the better performance. From the polarization curves we observe that the thinner membrane has a smaller slope and maintains its linearity up to higher current densities than the thicker membrane.



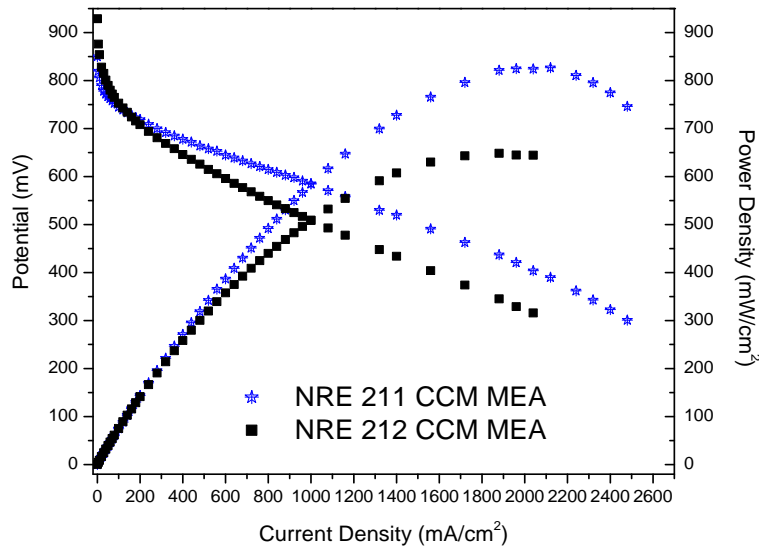


**Fig. 4.2 Polarisation and power density curves for PEMFCs with different membrane thickness**  
 ( $O_2$  flow rate = 2 l/min,  $H_2$  flow rate = 0.5 l/min,  $T_{cell} = 70^\circ C$ , atm)

This larger slope in thicker membranes is attributed to concentration overpotential and this loss of potential in the high current density region is due to mass transport limitations. Concentration overpotential arises when reactants aren't being supplied fast enough, this slows down the rate of the reaction, resulting in a decrease in cell potential. Because current density is directly proportional to the reaction rate, in the high current density region mass transport of reactants and products becomes the major limiting factor to cell potential. Thinner membranes will have better results due to their lower overall electrolyte resistance to proton transport.

#### ***4.1.3 Effect of operating pressure on cell performance***

The effect of operating pressure on the cell potential for a NRE 211 CCM MEA with a platinum loading of  $0.4 \text{ mg/cm}^2$  (anode and cathode) is shown in Figure 4.3 and Figure 4.4. We observe from Figure 4.3 that the cell potential increases with the cell operating pressure.

The results indicate that increasing the operating pressure from atmospheric pressure to 2 bar leads to a reduction in activation overpotential. The polarization curve at 2 bar also maintains its linearity up to higher current densities, which indicates that pressure also affects ohmic overpotential, because pressure will affect water flooding, and as a consequence ohmic overpotential is also affected. The increase in pressure results in an increase in gas solubility which would enhance the cell performance.

This can be explained by recalling that water is supplied to the membrane through the reactant gases that are saturated with vapour and by the water that is produced in the cell at the cathode side. Water is simultaneously transported via the electro-osmotic effect from the anode to the cathode along with protons that carry the current through the membrane [98], and this causes a higher accumulation of water on the cathode side compared to the anode. As a consequence, back diffusion of water from the cathode to the anode occurs, an occurrence which helps reduce problems related to membrane drying on the anode side and/or cathode flooding [99].

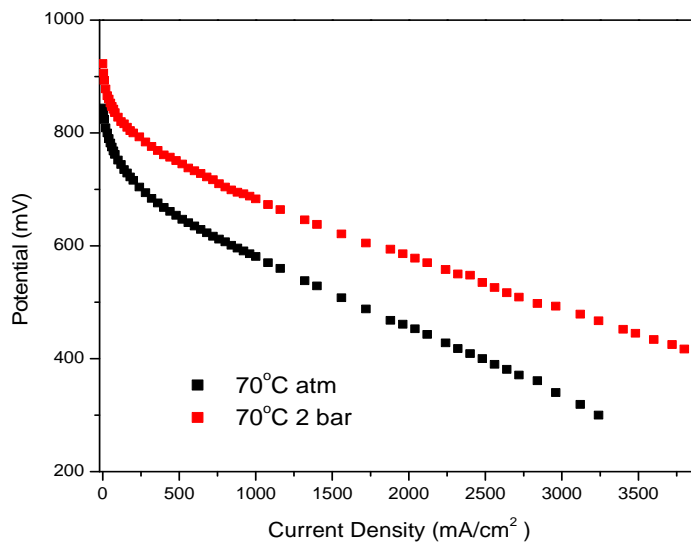


**Figure 4.3 Polarization curves for NRE 211 CCM MEAs illustrating the effect of pressure on cell performance.**

**Table 4.1:** Resistances of NRE 211 CCM MEA at different pressures, 0.1 mg/cm<sup>2</sup> Pt loading, 0.8 V cell voltage, 70 °C

	atm	2 bar
$R_{\Omega}$ (ohm)	0.02118	0.02095
$R_{ct}$ (ohm)	0.55882	0.2047

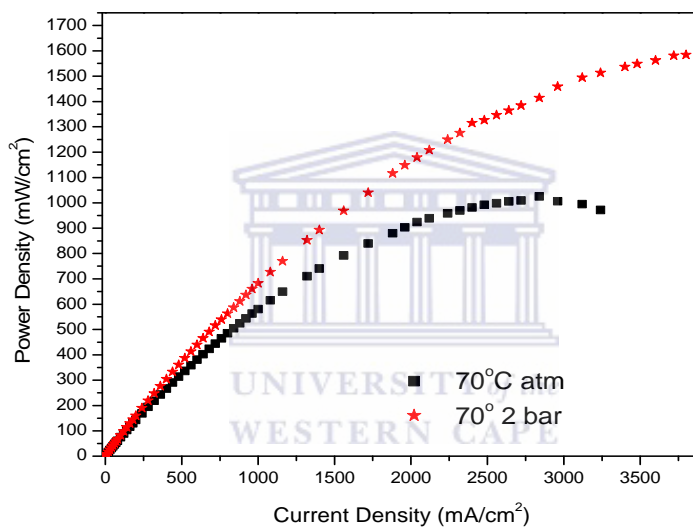


**Figure 4.4 Power Density curves for NRE 211 CCM MEA illustrating the effect of pressure on cell performance.**

A higher pressure results in a higher rate of gas diffusion through the electrodes and enhances cell performance. The power density curves in Figure 4.4 show that an increase in operating pressure from atmospheric pressure to 2 bar results in an increase in power density of approximately 560 mW/cm<sup>2</sup>.

Figure 4.5 shows the *in situ* impedance curves of a NRE 211 CCM MEA with a platinum loading of 0.8 V illustrating the effect of pressure on cell resistances. Single semicircular loops are observed in the Nyquist plot, this single semicircular loop is often referred to as the

"kinetic loop", indicating that the electrode processes are dominated by the interfacial kinetics of the ORR process [95]. The high frequency intercept (left side) of the impedance arc with the real axis represents the total ohmic resistance ( $R_{\Omega}$ ) of the cell, and the diameter of the kinetic loop, is a measure of the charge transfer resistance ( $R_{ct}$ ) of the ORR. This characteristic single loop provides information about the properties of the cathode, such as catalyst surface area, catalyst loading, and catalyst utilisation [100]. The low frequency intercept (right side) of the impedance arc with the real axis represents the polarization resistance of the cell, which include charge transfer and mass transfer resistance.

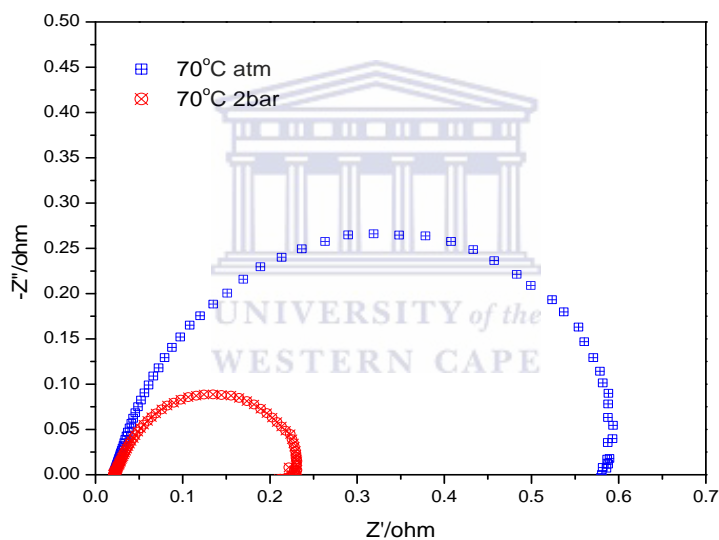


**Figure 4.5 *In situ* impedance curves of NRE 211 CCM MEA at different pressures, at a cell voltage of 0.8 V, 0.1 mg/cm<sup>2</sup> Pt loading (anode and cathode)**

From the impedance spectra in Figure 4.5 we observe that the diameter of the semicircle decreases significantly when going from atmospheric pressure to 2 bar back pressure. From the cell resistances tabulated in Table 4.1 we see that the charge transfer resistance is lower at higher operating pressures. The  $R_{ct}$  of 0.5588  $\Omega$  at atmospheric pressure, is significantly higher than the  $R_{ct}$  of 0.2047  $\Omega$  at a pressure of 2 bar. We can conclude that an increase in

pressure enhances the ORR in the catalyst layer, providing much faster reaction kinetics than can be attained at atmospheric pressure.

#### 4.1.4 Effect of operating temperature on cell performance

Figure 4.6 shows the performance of a CCM MEA at different cell temperatures. From the graph we observe that the performance increased with cell temperature over almost the entire current density range. The maximum power density reached was  $808 \text{ mW/cm}^2$ , this occurred at a cell temperature of  $80^\circ\text{C}$ . The current density and power density increased almost linearly with the cell temperature in the  $30\text{--}80^\circ\text{C}$  range. These results show that increasing the operating temperature had the effect of decreasing the cell polarization and hence increasing the cell performance. This temperature effect on cell performance can be explained by the more facile reaction kinetics at higher temperature for both the anode and the cathode, but in particular for the cathode, due to its slow ORR kinetics.

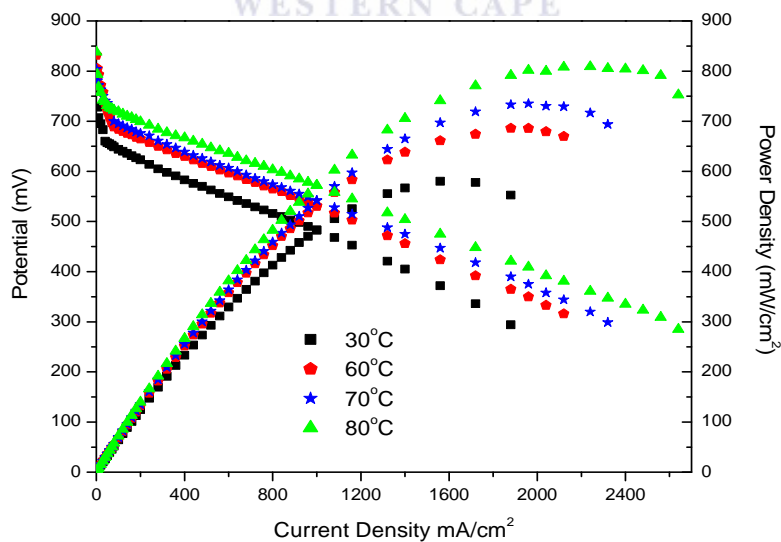
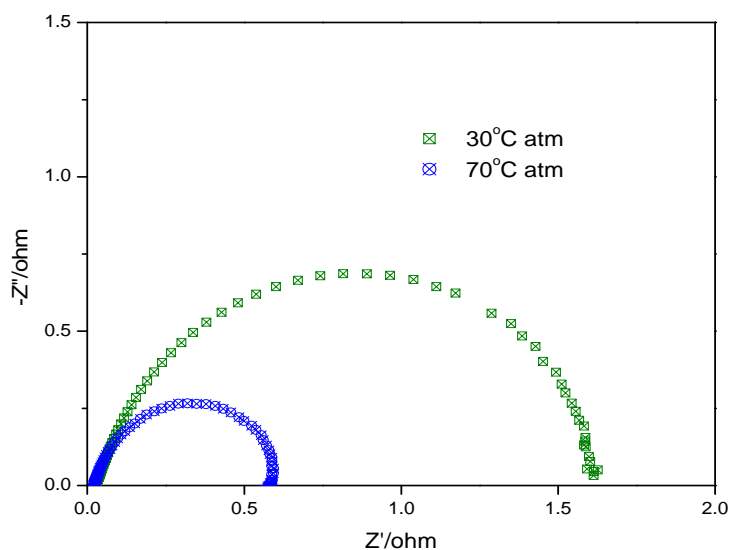
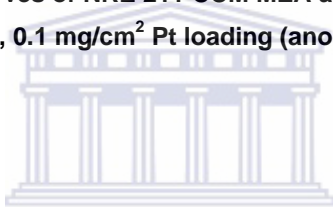


Figure 4.6 Effect of cell temperature on performance of NRE 211 CCM MEAs,  $0.05_a/0.1_c \text{ mg/cm}^2$  Pt loading



**Figure 4.7** *In situ* impedance curves of NRE 211 CCM MEA at different temperatures, at a cell voltage of 0.8 V, 0.1 mg/cm<sup>2</sup> Pt loading (anode and cathode)



**Table 4.2:** Resistances of NRE 211 CCM MEA at different temperatures, 0.1 mg/cm<sup>2</sup> Pt loading, 0.8 V cell voltage, atmospheric pressure

	30 °C	70 °C
<b>R<sub>Ω</sub> (ohm)</b>	0.0255	0.0212
<b>R<sub>ct</sub> (ohm)</b>	1.5875	0.5648

The impedance spectra in Figure 4.7 illustrates the effect increasing the operating temperature has on the cell resistances. We see that increasing the temperature to 70 °C results in a smaller semicircular loop, with the spectra showing improved ohmic and charge transfer resistances due to the improved reaction kinetics achieved by operating at higher temperature. An increase in temperature results in an increase in proton mobility, and as a

consequence the electrolyte membranes conductivity improves, therefore  $R_{\Omega}$  decreases as temperature increases. This increase in temperature also has the effect of increasing the activity of the gas molecules, this in turn will accelerate the transport of oxygen through the catalyst and diffusion layers, and as a result the mass transport resistance will decrease as the temperature increases.

Catalyst kinetics is improved at higher temperatures, which makes the charge transfer more facile, thus  $R_{ct}$  decreases as the temperature is increased. From the impedance curves in Figure 4.7 and the cell resistances tabulated in Table 4.2 we observe that the change in the extent of  $R_{ct}$  is larger than that of  $R_{\Omega}$  with increasing temperature. This indicates that operating temperature has a greater effect on the charge transfer resistance than on the cell resistance.

#### ***4.1.5 Performance of MEAs with different platinum loadings***

A series of MEAs were produced in which the catalyst layer was optimised by the gradual reduction of platinum loading on both the cathode and anode sides. Figure 4.8 shows the performance of five MEAs prepared with various platinum loadings. The platinum loadings on the anode and cathode sides, respectively were: (1) 0.4 mg/cm<sup>2</sup>; (2) 0.3 mg/cm<sup>2</sup>; (3) 0.2 mg/cm<sup>2</sup>; (4) 0.1 mg/cm<sup>2</sup>; (5) 0.05 mg/cm<sup>2</sup>.

We note that even when the platinum loadings were reduced from 0.4 to 0.05 mg/cm<sup>2</sup> the performance decline was slight. At low current density (<750 mA/cm<sup>2</sup>) we observe that as Pt loading increases, there is a slight increase in performance.

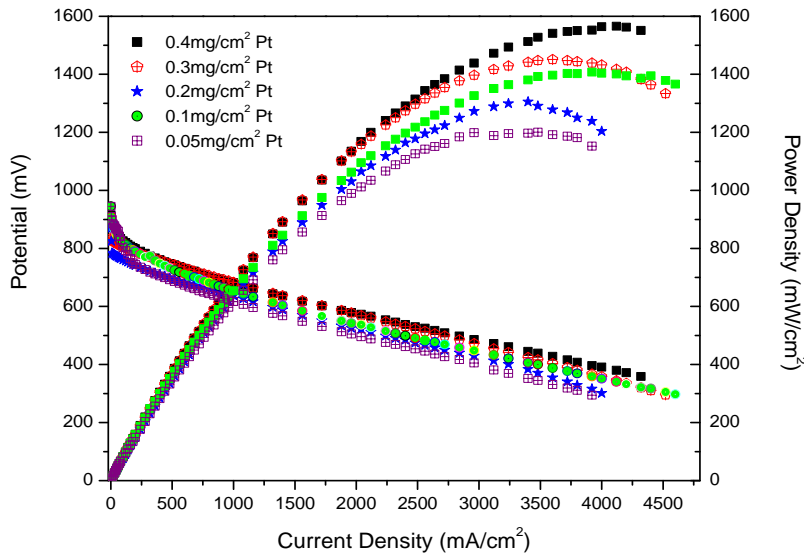


**Figure 4.8 Effect of platinum loading on performance of NRE 211 CCM MEAs prepared with several Pt contents and 15 wt.% Nafion<sup>®</sup> at 70 °C, 2 bar.**

We know that the linear decrease region of the polarisation curve is the result of ohmic overpotential, which originates from ionic flow through the electrolyte membrane and from electron flow through the electrode layers, flow field plates, and current collectors. From the polarisation curves we see that the MEAs have similar slopes which indicates that they had similar ohmic resistances. The fact that even the low platinum loading MEAs showed similar performance indicates that they had ample triple phase reaction boundaries and higher effective platinum utilisation.

The power density curves show that the maximum power density of 1.58 W/cm<sup>2</sup> was achieved by the MEA with a 0.4 mg/cm<sup>2</sup> Pt loading, and as expected the lowest power density of 1.2 W/cm<sup>2</sup> was achieved by the MEA with a 0.05 mg/cm<sup>2</sup> Pt loading. This ~0.38 W/cm<sup>2</sup> difference in cell performance is considered quite acceptable when one also considers the savings that would be made from the reduction in platinum loading.



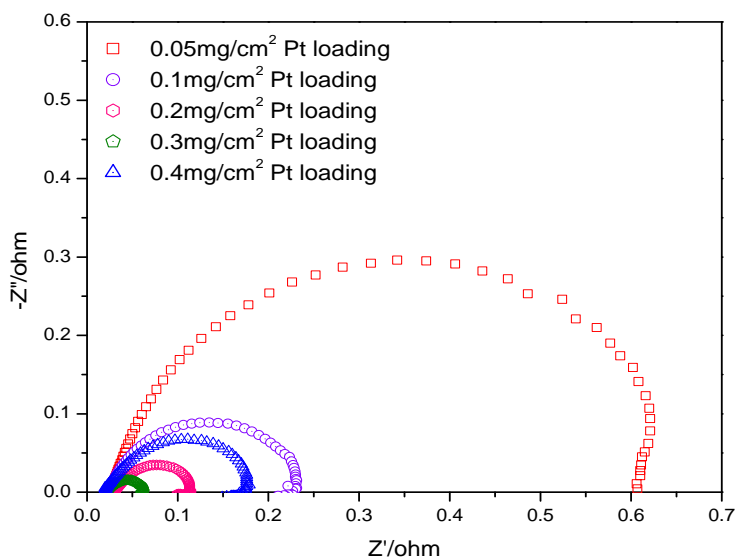


**Figure 4.9** *In situ* impedance curves of NRE 211 CCM MEAs with various Pt loadings, cell voltage of 0.8 V at 70 °C, 2 bar

We see from the impedance spectra in Figure 4.9 that the largest semicircular loop is observed for the MEA with the lowest platinum loading of 0.05 mg/cm<sup>2</sup>. This MEA also had the largest polarisation resistance and a  $R_{ct}$  value of 0.583 Ω, due to the low catalyst loading which causes slower ORR kinetics. We would expect the MEA with 0.4 mg/cm<sup>2</sup> platinum loading to exhibit the smallest semicircular loop as it has the highest catalyst loading, this is however not the case, as the smallest semicircular loop is observed for the MEA with 0.3 mg/cm<sup>2</sup> platinum loading. This could be due to the fact that even though the 0.4 mg/cm<sup>2</sup> MEA has a higher platinum loading, it does not necessarily have a higher effective catalyst surface area. The 0.3 mg/cm<sup>2</sup> showed the smallest  $R_{ct}$  of 0.04 Ω, which implies that the MEA has increased platinum utilisation even though it has less catalyst than 0.4 mg/cm<sup>2</sup> Pt loading MEA. This also shows that the 0.3 mg/cm<sup>2</sup> MEA has fewer mass transport limitations than the 0.4 mg/cm<sup>2</sup> MEA as a consequence of its thinner catalyst layer. An optimal catalyst layer

thickness with an optimum between mass transport limitation and reaction sites is achieved by the 0.3 mg/cm<sup>2</sup> MEA.

The 0.04 mg/cm<sup>2</sup> MEA did however, have the lowest  $R_{\Omega}$  of 0.0198  $\Omega$  which may be due to the fact that a higher catalyst loading results in a greater amount of Pt particles which means that electrocatalysis is more rapid. This results in an increase flow of protons through the electrolyte membrane, and since protons drag water molecules along with them through the membrane (electro-osmotic effect), the resulting concentration gradient leads to back diffusion from the cathode to the anode, thus membrane hydration is increased which leads to a decrease in the ohmic resistance.

**Table 4.3:** Cell resistances of various Pt loading NRE 211 CCM MEAs, at different temperatures and pressures, at a cell voltage of 0.8 V

Operating conditions	0.05 mg/cm <sup>2</sup>		0.05 <sub>a</sub> /0.1 <sub>c</sub> mg/cm <sup>2</sup>		0.1 mg/cm <sup>2</sup>		0.2 mg/cm <sup>2</sup>		0.3 mg/cm <sup>2</sup>		0.4 mg/cm <sup>2</sup>	
	$R_{\Omega}$ (ohm)	$R_{ct}$ (ohm)	$R_{\Omega}$ (ohm)	$R_{ct}$ (ohm)	$R_{\Omega}$ (ohm)	$R_{ct}$ (ohm)	$R_{\Omega}$ (ohm)	$R_{ct}$ (ohm)	$R_{\Omega}$ (ohm)	$R_{ct}$ (ohm)	$R_{\Omega}$ (ohm)	$R_{ct}$ (ohm)
30 °C atm	0.0286	1.547	0.0294	3.781	0.0255	1.588	0.0282	0.3062	0.0250	0.2126	0.0236	1.0214
70 °C atm	0.0229	1.593	0.0221	0.635	0.0212	0.5648	0.0377	0.2849	0.0209	0.0624	0.0193	0.381
70 °C 2 bar	0.0274	0.583	0.0204	0.152	0.0209	0.2047	0.0291	0.0854	0.0217	0.04	0.0198	0.1521

#### 4.1.6 Effect of cathode platinum loading on cell performance

In order to evaluate the effect ORR kinetics has on PEMFC performance, two MEAs having the same anode loadings but different cathode loadings were prepared. Figure 4.10 shows a comparison of these MEAs having platinum loadings of: (1) 0.05 mg/cm<sup>2</sup> for the anode and cathode; (2) 0.05 mg/cm<sup>2</sup> (anode) and 0.1 mg/cm<sup>2</sup> (cathode).

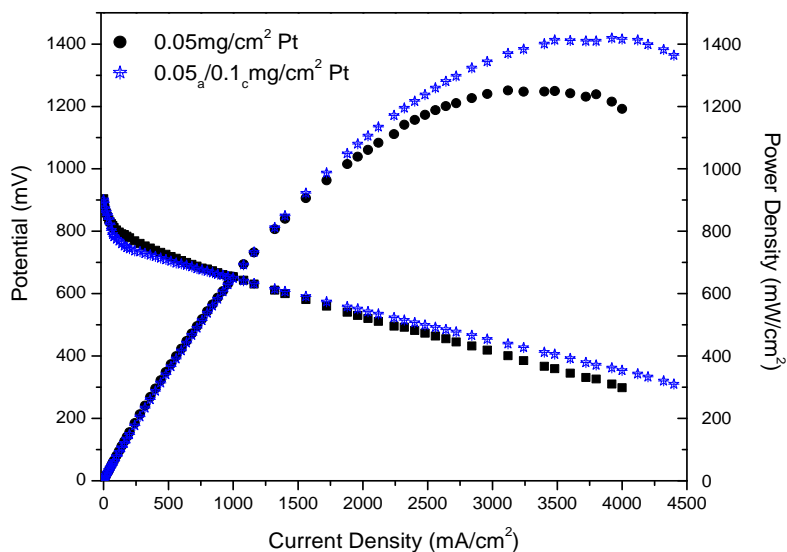


**Figure 4.10 Effect of cathode platinum loading on performance of NRE 211 CCM MEAs prepared with 15 wt.% Nafion® at 70 °C, 2 bar.**

As can be seen from the polarisation curves; increasing the platinum loading on the cathode side has the effect of enhancing the performance in the middle to high current density region (1250-4500 mA/cm<sup>2</sup>), allowing the fuel cell to reach a higher performance. This shows that increasing the cathode platinum loading slightly has a significant effect in improving cell performance by improving the rate of the oxygen reduction reaction.

Since the ORR kinetics is a limiting factor in PEM fuel cell performance, it follows that the cathode should have a higher platinum loading than the anode. An increase in platinum amount on the cathode has the effect of increasing the active area and improving performance by providing faster cathode reaction kinetics.

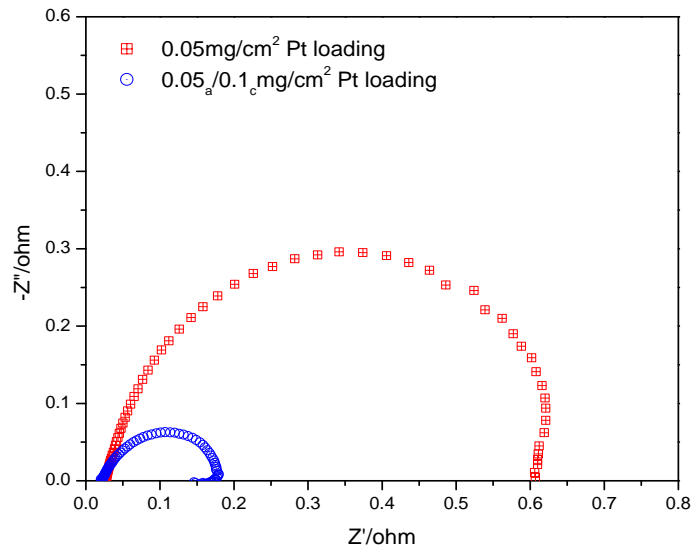


**Figure 4.11** *In situ* impedance curves for NRE 211 CCM MEAs having different cathode platinum loadings, cell voltage of 0.8 V at 70 °C, 2 bar

**Table 4.4:** Resistances of NRE 211 CCM MEAs, cathode platinum loading effect, at a cell voltage of 0.8 V, at 70 °C, 2 bar

	0.05 mg/cm <sup>2</sup>	0.05 <sub>a</sub> /0.1 <sub>c</sub> mg/cm <sup>2</sup>
<b>R<sub>Ω</sub> (ohm)</b>	0.0274	0.0204
<b>R<sub>ct</sub> (ohm)</b>	0.583	0.152

The impedance curves in Figure 4.11 we see that increasing the catalyst loading on the cathode has the effect of decreasing the size of the kinetic loop, and from the resistances tabulated in Table 4.4 we see that the ohmic and charge transfer resistance decreases as the cathode loading is increased. Although both the  $R_{\Omega}$  and  $R_{ct}$  values decrease, the  $R_{ct}$  shows a greater improvement than the  $R_{\Omega}$ . This is an expected result as charge transfer resistance has a direct relation to the slow ORR kinetics at the cathode, this reaction kinetics is improved by

the higher platinum loading, which improves the catalyst surface area. The ohmic resistance, on the other hand, is mainly affected by the membrane resistance which is related to membrane hydration.

#### 4.1.7 Effect of Nafion<sup>®</sup> content in the catalyst layer

Since Nafion<sup>®</sup> is an important constituent in the catalyst layers, helping to increase the triple phase reaction boundaries and increasing platinum utilisation in the electrode. Nafion<sup>®</sup> is hydrophilic in nature and aids in maintaining membrane hydration, especially at high current densities where membrane dehydration becomes a problem. It also affects gas permeability, catalytic activity, and ionic resistance in the electrodes [101]. Nafion<sup>®</sup> content therefore needs to be optimised in order to achieve the correct balance among these influencing factors and thereby obtaining high performance MEAs [102-104].

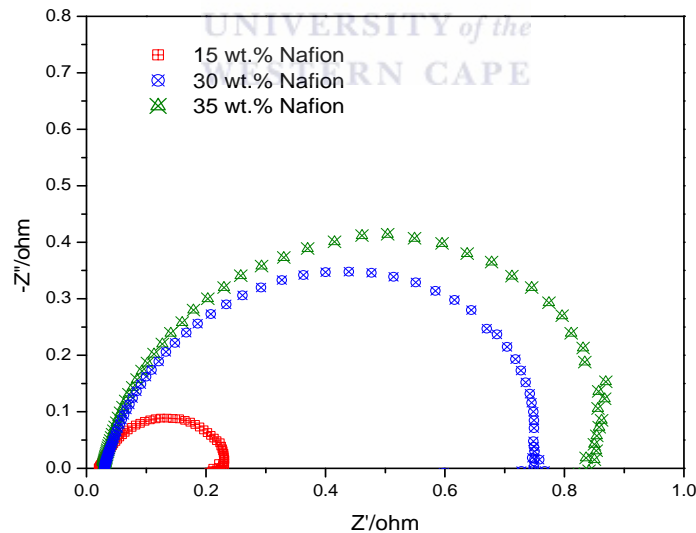


**Figure 4.12** *In situ* impedance curves of NRE 211 CCM MEAs with various Nafion<sup>®</sup> content at a cell voltage of 0.8 V, 0.1 mg/cm<sup>2</sup> Pt loading (anode and cathode) at 70 °C, 2 bar

EIS was used to investigate the effect of Nafion<sup>®</sup> in the catalyst layer. It was discovered that the amount of Nafion<sup>®</sup> in the catalyst layer strongly influences the resistance and hence performance of MEAs. From Figure 4.12 we can calculate the ohmic and charge transfer resistance; the cell resistances are tabulated in Table 4.5. The impedance spectra show that the MEAs with 15, 30, and 35 wt.% Nafion<sup>®</sup> in the catalyst layer showed ohmic resistances of 0.0209  $\Omega$ , 0.0283  $\Omega$ , and 0.0301  $\Omega$  respectively. The 15 wt.% MEA showed the smallest ohmic resistance, which can be attributed to improved contact and ionic flow through the electrolyte membrane. This effect does, however, have a limit as can be seen by the higher resistance of the 30 and 35 wt.% Nafion<sup>®</sup> MEAs.

**Table 4.5:** Resistances of single cells with various NRE 211 CCM MEAs, 0.1 mg/cm<sup>2</sup> Pt at 70 °C, 2 bar

	15 wt. %	30 wt. %	35 wt. %
<b>R<sub>Ω</sub> (ohm)</b>	0.0209	0.0283	0.0301
<b>R<sub>ct</sub> (ohm)</b>	0.2047	0.8074	0.7208

We also observe that the 15 wt.% Nafion<sup>®</sup> MEA had a charge transfer resistance of 0.2047  $\Omega$ , whereas the 30 and 35 wt.% Nafion<sup>®</sup> MEAs showed charge transfer resistances of 0.8074  $\Omega$  and 0.7208  $\Omega$  respectively. This implies that the MEA with 15 wt.% Nafion<sup>®</sup> loading in the catalyst layer provides a higher available and more conductive catalyst surface area, it thus enhances the triple phase boundary region allowing the electrochemical reactions to proceed swiftly. The larger loops of the MEAs with 30 and 35 wt.% Nafion<sup>®</sup> shows that although the ionomer is beneficial in improving proton conductivity, too much Nafion<sup>®</sup> in the catalyst layer is not advantageous for the electronic conductivity and hinders the transport of

oxygen. This can be attributed to the increase in distance through which the gas has to permeate, diffuse, or migrate to the catalyst surface, as some catalyst sites may be covered by a thick layer of Nafion<sup>®</sup> which may render them inactive.

From the impedance results we can conclude that the MEA with 15 wt.% Nafion<sup>®</sup> content in the catalyst layer showed the best conductivity, exhibiting the least ohmic and charge transfer resistances.

#### 4.1.8 The influence of cell voltage

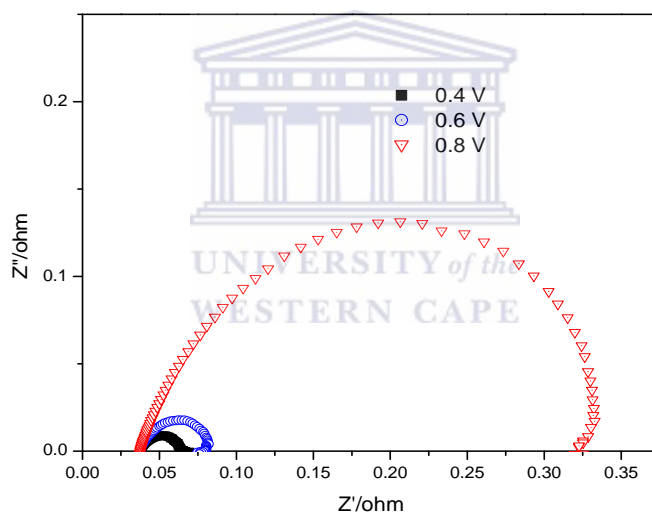


**Figure 4.13** *In situ* impedance curves of NRE 211 CCM MEA at various cell voltages, 0.2 mg/cm<sup>2</sup> Pt loading (anode and cathode), 70 °C atm

We notice from Figure 4.13 that the size of the semicircular loop decreases as cell voltage decreases. The cell resistances tabulated in Table 4.6 shows that the ohmic resistances are practically the same at various cell voltages, this is however, not the case for the charge transfer resistance. The  $R_{ct}$  increases as cell voltage increases, this is due to the tendency of

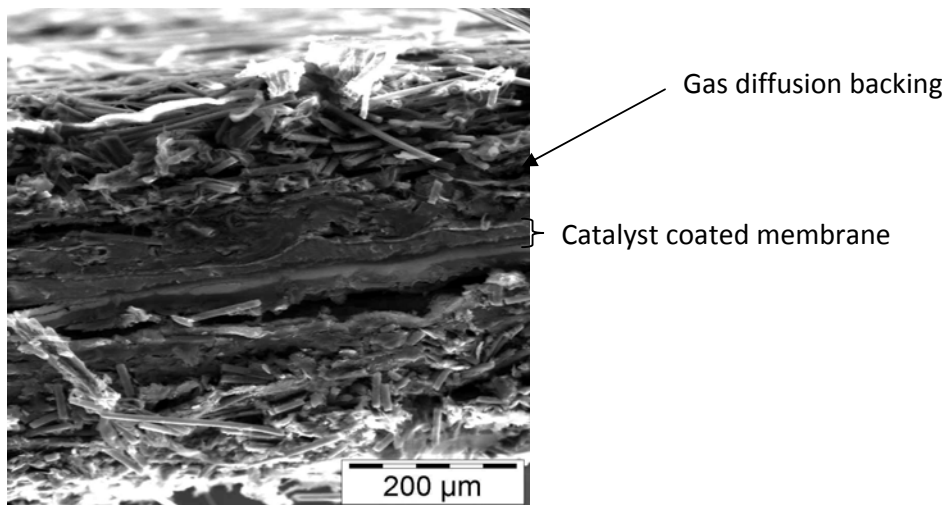
$R_{ct}$  to decrease with increasing current because of the increased driving force for the electrode processes.

**Table 4.6:** Resistances of NRE 211 CCM MEA at different cell voltages, 0.2 mg/cm<sup>2</sup> Pt loading, 70 °C atm

	$R_{\Omega}$ (ohm)	$R_{ct}$ (ohm)
<b>0.4 V</b>	0.0376	0.0269
<b>0.6 V</b>	0.0373	0.0421
<b>0.8 V</b>	0.0377	0.2853

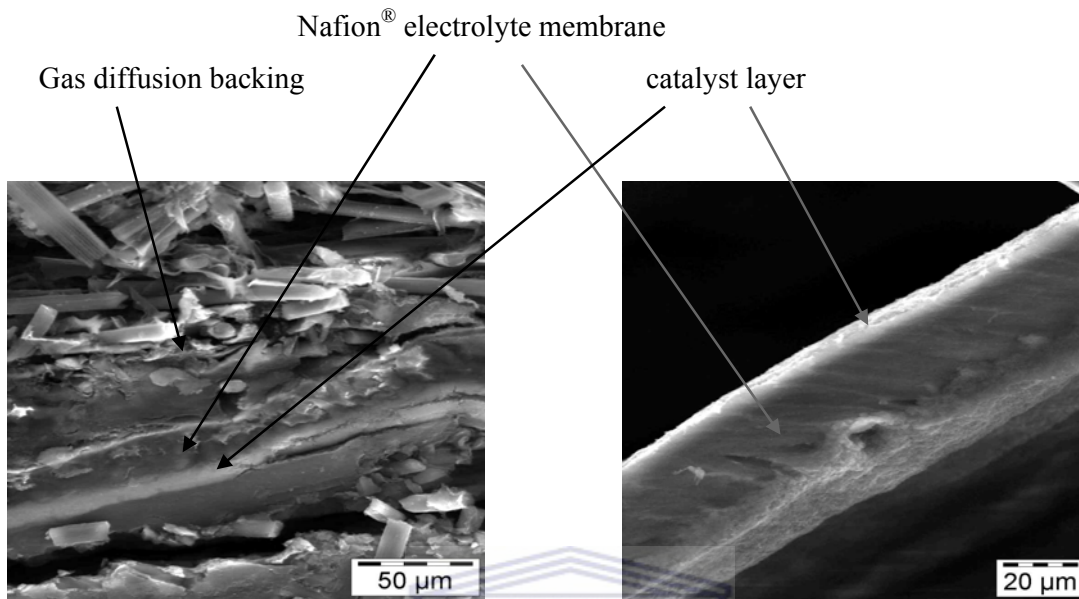
#### 4.2 The morphology of CCM MEA

Figure 4.14 shows a cross-sectional SEM image of a CCM MEA, in which we can clearly observe the gas diffusion layer and the CCM. Different parts of the CCM MEA are seen clearly in Figures 4.15; we are able to discern the anode and cathode catalyst layers, the Nafion<sup>®</sup> electrolyte membrane, and the gas diffusion backings which face each catalyst layer.



**Figure 4.14** SEM image of a cross-section of a CCM MEA at 200 X magnification





**Figure 4.15 SEM image of a cross-section of a CCM MEA at 600 x magnification**

**Figure 4.16 SEM image of a cross-section of a CCM at 1000 x magnification**

Figure 4.16 shows a cross-sectional SEM image of just a CCM, here we are able to see the close contact between the catalyst layers and the electrolyte membrane, which is one of the reasons for good performance achieved by the CCM MEAs. The thickness of the catalyst layers for this CCM was approximately  $3.6\ \mu\text{m}$ , such thin catalyst layers make smaller mass transfer and charge transfer resistances possible. The SEM image also shows the uniform catalyst layer, which allows for the achievement of a higher utilisation of catalyst particles.

The combination of the thin catalyst layers, close contact between catalyst layers and electrolyte membrane, and the uniformity of the catalyst layer structure is in all likelihood the main reason for the high performance achieved by the CCM MEAs prepared and tested during this research.

## Chapter 5: Conclusion and recommendations

### 5.1 Conclusions

MEAs with reduced platinum loadings were successfully prepared and optimised using the CCM method for electrode fabrication. Following a literature survey and experimental evaluations, the CCM method explained here was used for all MEA preparations. This method involves less preparation steps as the electrolyte membrane is not chemically treated before being used. In addition to this, ultrasonication was found to be sufficient for the dispersion of catalyst and GDL particles in prepared inks, with preparation time being significantly shortened by excluding the mechanical agitation step reported in literature [83].

The performance of the CCM MEAs were evaluated by performing polarisation studies on a single cell with an active area of 5 cm<sup>2</sup>. As expected Nafion<sup>®</sup> NRE 211 membranes was found to be the optimum Nafion<sup>®</sup> membrane for CCM MEAs, as it showed improved performance over CCM MEAs prepared with Nafion<sup>®</sup> NRE 212 membranes. This was expected as literature has shown that membrane resistance decreases with decreasing membrane thickness.

The CCM method of MEA fabrication showed significant improvement in performance when compared to the GDL-based method of MEA fabrication, with the 0.4 mg/cm<sup>2</sup> Pt loading (anode and cathode) CCM MEA exhibiting improved performance over the GDL-based MEA with the same Pt loading in the high current density region. This can be attributed to the improved interfacial contact between electrolyte and catalyst layers in the CCM MEA, leading to improved mass transport of reactants especially at higher current densities.

The optimum reaction temperature and pressure for improved cell performance was shown to be an operating temperature of 70 °C, with the application of 2 bar back-pressure. Higher

operating temperatures and pressures improves reaction kinetics, however, we must also take into account the effect these operating conditions will have on the entire fuel cell system so we cannot limitlessly keep increasing the operating conditions.

Optimum Nafion<sup>®</sup> ionomer loading in the catalyst was shown to be 15 wt.%, impedance analysis showed that this loading had the smallest kinetic loops when compared to 30 wt.% and 35 wt.%, this differs from literature as some say 30 wt.% Nafion<sup>®</sup> is the optimum value.

The platinum loading in the catalyst layer of the CCMs was successfully reduced from 0.4-0.05 mg/cm<sup>2</sup> with losses of ~0.38 W/cm<sup>2</sup> in power density, which is acceptable if one considers that material costs have been reduced by decreasing the amount of catalyst required to 12.5% of its initial value. Even this ~0.38 W/cm<sup>2</sup> loss in power density could be overcome by increasing the platinum loading on the cathode electrode to 0.1 mg/cm<sup>2</sup>, while the anode platinum loading remains unchanged at 0.05 mg/cm<sup>2</sup>. This results in a power density of 1.419 W/cm<sup>2</sup>, which is only a loss of ~0.161 W/cm<sup>2</sup> from the 1.58 W/cm<sup>2</sup> produced by the 0.4 mg/cm<sup>2</sup> Pt loading (anode and cathode) MEA. A catalyst reduction to 18.75 % of the initial value is still an acceptable catalyst reduction considering the gain in performance obtained.

The impedance analysis confirmed that CCM MEAs provide high platinum utilisation, and that even low Pt loading CCM MEAs can have sufficient Pt catalyst for a highly effective surface area. SEM analysis proved that the CCM method can produce MEAs with uniform catalyst layers, which are in close contact with the electrolyte membrane.

## ***5.2 Recommendations***

Some recommendations for future work on this research are suggested below:

- Further work should be performed on optimisation of the GDL structure, as this also forms an essential part of the MEA structure.

- Different electrolyte membranes should be tested and prepared and their performance compared with that of Nafion<sup>®</sup> electrolyte membrane.
- Durability tests should be performed on these CCM MEAs as the electrolyte membranes used here are extremely thin (in the order of 25 and 50  $\mu\text{m}$  thick), and long-term durability is a key parameter, especially when considering transport applications.



## References

1. M. Ball, M. Wietschel, *International Journal of Hydrogen Energy*, (2008), doi:10.1016/j.ijhydene.2008.11.014.
2. S. Haile, S.M. Kauzlarich, P. Battle, J. Greedan, *Chemistry of Materials*, 22 (2010) 585-586.
3. D.L. Stojić, M.P. Marčeta, S.P. Sovilj, Š.S. Miljanić, *Journal of Power Sources*, 118 (2003) 315-319.
4. B.P. Tarasov and M.V. Lototskii, *Russian Journal of General Chemistry*, 77 ( 2007) 660-675.
5. <http://www1.eere.energy.gov/hydrogenandfuelcells/animation/mod1.html>
6. [http://www.h-tec.com/html/web/education/english/technologie\\_verbraucher.asp?id=315](http://www.h-tec.com/html/web/education/english/technologie_verbraucher.asp?id=315)
7. E. Rasten, *Electrocatalysis in water electrolysis with solid polymer electrolyte*, Ph.D. thesis, Norwegian University of Science and Technology (2001).
8. M. Winter, R.J. Brodd, *Chemical Reviews*, 104 (2004) 4245-4269.
9. Kirk-Othmer *Encyclopedia of Chemical Technology*, John Wiley & Sons, Inc . Vol 12, 5th Edition, 2005.
10. P. Boulanger, M. Perrin, *Storage Technology Report WPST5: Electrolyser, hydrogen storage and Fuel-cell*, Investire-Network, 2003.
11. M.S. Whittingham, R.F. Savinell, T. Zawodzinski, *Chemical Reviews*, 104 (2004) 4243-4244.
12. G.Hoogers, "Fuel Cell Technology Handbook", CRC Press: Boca Raton, FL, 2003.
13. S. M. Haile, *Acta Materials*, 51 (2003) 5891-6000.
14. K.V. Kordesch, G.R. Simader, *Chemical Reviews*, 95 (1995) 191-207.
15. R. George, A.C. Casanova, S. Veyo, *Statuses of Siemens Westinghouse SOFC Program. Extended Abstracts of the 2002 Fuel Cell Seminar*. Washington DC: Courtesy Associates, Inc., 2002
16. B.C.H Steele, *Nature*, 400 (1999) 619.
17. A. L. Dicks, *Current Opinion in Solid State and Materials Science*, 8 (2004) 379-383.
18. M. Bischoff, *Journal of Power Sources*, 160 (2006) 842-845.
19. "Fuel Cell Handbook", seventh edition, EG & G Technical Services, Inc., U.S. Department of Energy, Office of Fossil Energy, National Energy Laboratory, 2004.

20. S. Randström, C. Lagergren, P. Capobianco, *Journal of Power Sources*, 160 (2006) 782-788.
21. N. Sammes, R. Bove, K. Stahl, *Current Opinion in Solid State and Materials Science*, 8 (2004) 372-378.
22. A. Kirubakaran, S. Jain, R.K. Nema, *Renewable and Sustainable Energy Reviews*, 13 (2009) 2430-2440.
23. L. Larmine, A. Dicks, *Fuel cells systems explained*, UK: John Wiley and Sons Ltd; 2000.
24. H. Shiota, K. Mitsuda, J. Aragane, T. Murachashi, In *Proceedings of The Electrochemical Society Fall Meeting*, Hollywood, FL, USA, 15-20 October, 1989, Extended Abstracts, Abstract No. 88
25. J.M.F. Ferreira, H.M.M. Diz, *Journal of Hard Materials*, 3 (1992) 17-27.
26. S. Dheenadayalan, R. Song, D. Shin, *Journal of Power Sources*, 107 (2002) 98-102.
27. E. Passalacqua, P.L. Antonucci, M. Vivaldi, A. Patti, V. Antonucci, N. Giordano, K. Kinoshita, *Electrochimica Acta*, 37 (1992) 2725-2730.
28. A. Hamnett, *Catalysis Today*, 38 (1997) 445-457.
29. L. Zhong, X. Wang, Y. Jiang, O. Zhong, X. Qiu, Y. Zhou, et al., *Sensors and Actuators A: Physical*, 143 (2009) 70-76.
30. S.K. Kamarudin, F. Achmad, W.R.W. Daud, *International Journal of Hydrogen Energy*, 34 (2009) 6902-6916.
31. R.Z. Jiang, D. Chu, *Journal of Electrochemical Society*, 151 (2004) 69-76.
32. J.G. Liu, T.S. Zhao, Z.X. Liang, R. Chen, *Journal of Power Sources*, 153 (2006) 61-67.
33. J.B. Goodenough, R. Manoharan, A.K. Shukla, K.V. Ramesh, *Chemistry of Materials*, 1 (1989) 391.
34. P.K. Das, X. Li, Z. Liu, *Journal of Electroanalytical Chemistry*, 604 (2007) 72-90.
35. B. Smitha, S. Sridhar, A.A. Khan, *Journal of Membrane Science*, 259 (2005) 10-26.
36. T. Zawodzinski, J. Davey, J. Valerio, S. Gottesfeld, *Electrochimica Acta*, 40 (1995) 297-302.
37. H.A. Gasteiger, J.E. Panels, S.G. Yan, *Journal of Power Sources*, 127 (2004) 162-171.
38. S.K. Kamarudin, W.R.W. Daud, S.L. Ho, U.A. Hasran, *Journal of Power Sources*, 163 (2007) 743-754.
39. L. Carrette, K.A. Friedrich, U. Stimming, *Fuel Cells*, 1 (2001) 1-39.
40. L.K. Verma, *Journal of Power Sources*, 86 (2000) 464 -468.

41. B.V. Mathiesen, M.P. Nielsen, "The nature of fuel cells", Department of Development and Planning, Aalborg University, (2008)
42. A. Kusko, "Emergency/Standby Power Systems," McGraw-Hill Book Company, 1989, ISBN: 0-07-035688-0
43. Hydrogen Fuel Cells: Research Progress and Near-Term Opportunities, Christy Cooper, US Department of Energy Hydrogen Program, Washington, DC <http://wstiac.alionscience.com/quarterly>
44. K. Rajashekara, "Propulsion System Strategies for Fuel Cell Vehicles", Fuel Cell Power for Transportation 2000 Conference, SAE 2000 World Congress, March 2000, Ref: 2000-01-0369.
45. T. Matsumoto, et al., "Development of Fuel Cell Hybrid Vehicle", Fuel Cell Power for Transportation 2002 Conference, SAE 2002 World Congress, March 2002, Ref: 2002-01-0096.
46. B. Zhou, W. Huang, Y. Zong, A. Sobiesiak, Journal of Power Sources, 155 (2006) 190-202.
47. M. Mikkola, Experimental studies on Polymer Electrolyte Membrane Fuel Cell Stacks, M.Sc. thesis, Helsinki University of Technology, Department of Engineering Physics and Mathematics, (2001).
48. M. Hu, S. Sui, X. Zhu, Q. Yu, G. Cao, X. Hong, H. Tu, International Journal of Hydrogen Energy, 31 (2006) 1010-1018.
49. S.O. Morner, S.A. Klein, Journal of Solar Energy Engineering, 123 (2001) 225–231.
50. S. Giddey, F.T. Ciacchi, A.P.S. Badwal, Journal of Power Sources, 125 (2004) 155–165.
51. M.H. Tsai, Y.Y. Yan, H.S. Chu, R.J. Shyu, F. Tsau, Analysis of a 3 kW PEM fuel cell stack developed by ITRI, 2nd International Conference on Fuel Cell Science, Engineering Technology, (2004) 201–204.
52. J. Scholta, N. Berq, P. Wilde, L. Jorissen, J. Garche, Development and performance of a 10kW PEMFC stack, Journal of Power Sources, 127 (2004) 206-212.
53. E.A. Cho, U.-S. Jeon, S.-A. Hong, I.-H. Oh, S.-G. Kang, Journal of Power Sources, 142 (2005) 177-183.
54. M. Santis, D. Schmid, M. Ruge, S. Freunberger, F.N. Büchi, Fuel Cells, 4 (2004) 214-218.

55. F. Barbir, M. Fuchs, A. Husar, J. Neutzler, Design and operational characteristics of automotive PEM fuel cell stacks, Fuel cell power for transportation, SAE SP-1505, SAE, Warrendale, PA; 2000 p. 63-69.
56. Y.A. Dobrovolskii, E.V. Volkov, A.V. Pisareva, Y.A. Fedotov, D.Y. Likhachev, and A. L. Rusanov, Russian Journal of General Chemistry, 77 (2007) 766-777.
57. K.D. Kreuer, Journal of Membrane Science, 185 (2001) 29.
58. J.E. Hensley, J.D. Way, S.F. Dec, K.D. Abney, Journal of Membrane Science, 298 (2007) 190-201.
59. A. Appleby, F. Foulkes, "Fuel Cell Handbook", Van Nostrand Reinhold, New York, USA (1989), ISBN 00-442-3126-6
60. S. Tominaka, C. Wu, K. Kuroda, T. Osaka, Journal of Power Sources, 195 (2010) 2236-2240.
61. M. Wilson, S. Gottesfield, Journal of Applied Electrochemistry, 22 (1992) 1-7.
62. J.W. Weidner, V.A. Sethuraman, and J.W. Van Zee, Engineering a Membrane Electrode, The Electrochemical Society Interface (2003) 40-43.
63. D. Davies, P. Adcock, M. Turpin, S. Rowen, Journal of Power Sources, 86 (2000) 237-242.
64. D. Davies, P. Adcock, M. Turpin, S. Rowen, Journal of Applied Electrochemistry, 30 (2000) 101-105.
65. R. Makkus, A. Janssen, F. de Bruijn, R. Mallant, Journal of Power Sources, 86 (2000) 274-282.
66. F. Barbir, J. Braun, J. Neutzler, Effect of Collector Plate Resistance on Fuel Cell Stack Performance, in Proton Conducting Membrane Fuel Cells II, Proc. Vol. 98-27, pp. 400-406, The Electrochemical Society, Pennington, N.J., 1999.
67. T. Besmann, J. Klett, J. Henry Jr., E. Lara-Curzio, Journal of Electrochemical Society, 147 (2000) 4083-4086.
68. D. Busick, M. Wilson, Low-Cost Composite Bipolar Plates for PEFC Stacks, in Proton Conducting Membrane Fuel Cells II, Proc. Vol. 98-27, pp. 435- 445, The Electrochemical Society, Pennington, N.J., 1999.
69. J.C. Amphlett, M. Farahani, R.F. Mann, B.A. Peppley, P.R. Roberge, in Proceedings of the 26th Intersociety Energy Conversion Engineering Conference, August 4-9, 1991, Volume 3, Conversion Technologies/Electrochemical Conversion, American Nuclear Society, La Grange, Illinois, p. 624, 1991.



70. "Fuel Cell Handbook", 5th edition, EG & G Services, Parsons Inc, Science Applications International Corporation, U.S. Department of Energy, Office of Fossil Energy, National Energy Technology Laboratory, Morgantown, West Virginia, October 2000.
71. W. Dai, H. Wang, X.-Z. Yuan, J.J. Martin, D. Yang, J. Qiao, J. Ma, International Journal of Hydrogen Energy, 34 (2009) 9461-9478.
72. J. Yi, T. Nguyen, An along the channel model for proton exchange membrane fuel cells, Journal of Electrochemical Society, 145 (1998) 1149-1159.
73. X.H. Ye, C.Y. Wang, Journal of Electrochemical Society, 154 (2007) 683-686.
74. D. Rivin, C.E. Kendrick, P.W. Gibson, N.S. Schneider, Polymer, 42 (2001) 623-635.
75. M.M. Mench, Q.L. Dong, C.Y. Wang, Journal of Power Sources, 124 (2003) 90-98.
76. S. Vengatesan, H. J. Kim, E.A. Cho, S.U. Jeong, H.Y. Ha, I.H. Oh, et al., Journal of Power Sources, 156 (2006) 294-299.
77. M.B. Ji, Z.D. Wei, S.G. Chen, L. Li, Journal of Physical Chemistry, 113 (2009) 765-771.
78. S.-J. Shin, J.-K. Lee, H.-Y. Ha, S.-A. Hong, H.-S. Chun, I.-H. Oh, Journal of Power Sources, 106 (2002) 146-152.
79. S. Lister, G. McLean, Journal of Power Sources, 130 (2004) 61-76.
80. S.D. Thompson, L.R. Jordan, M. Forsyth, Electrochimica Acta, 46 (2001) 1657-1663.
81. M. Pan, H. Tang, S. Mu, R. Yuan, J. Mater. Res. 19 (2004) 2279-2284.
82. E. Antolini, L. Giorgi, A. Pozio, E. Passalacqua, Journal of Power Sources 77 (1999) 136-142.
83. Z. Qi, A. Kaufman, Journal of Power Sources, 113 (2003) 37-42.
84. P. Gode, F. Jaouen, G. Lindbergh, A. Lundblad, G. Sundholm, Electrochimica Acta, 48 (2003) 4175-4187.
85. T. Frey, M. Linardi, Electrochimica Acta, 50 (2004) 99-105.
86. Y. Zhang, C. Wang, N. Wan, Z. Liu, Z. Mao, Electrochemistry Communications, 9 (2007) 667-670.
87. H. Tang, S. Wang, S.P. Jiang, M. Pan, Journal of Power Sources, 170 (2007) 140-144.
88. X. Cheng, B. Yi, M. Han, J. Zhang, T. Qiao, J. Yu, Journal of Power Sources, 79 (1999) 75-81.
89. H.A. Gasteiger, S.S. Kocha, B. Sompalli, F.T. Wagner, Applied Catalysis B: Environmental, 56 (2005) 9-35.
90. K. Sawai, N. Suzuki, Journal of Electrochemistry Society, 151 (2004) 2132-2137.

91. H. Zhong, H. Zhang, G. Liu, Y. Liang, J. Hu, B. Yi, *Electrochemistry Communications*, 8 (2006) 707-712.
92. E.J. Taylor, E.B. Anderson, N.R.K. Vilambi, *Journal of Electrochemistry Society*, 139 (1992) L45-L46.
93. S. Hirano, J. Kim, S. Srinivasan, *Electrochimica Acta*, 42 (1997) 1587-1593.
94. N. Cunningham, E. Irissou, M. Lefevre, M.C. Denis, D. Guay, J.P. Dodelet, *Electrochemistry Solid-State Letters*, 3 (2003) A125-A128.
95. M.K. Debe, T.N. Pham, A.J. Steinbach, US Patent 97,948,851 (1999).
96. R. Benitez, J. Soler, L. Daza, *Journal of Power Sources*, 151 (2005) 108-113.
97. Y.-H. Cho, H.-S. Park, Y.-H. Cho, D.-S. Jung, H.-Y. Park, Y.-E. Sung, *Journal of Power Sources*, 172 (2007) 89-93.
98. D. Bessarabov, *Membrane Technology*, 2009 (2009) 6-12.
99. X. Yuan, H. Wang, J.C. Sun, J. Zhang, *International Journal of Hydrogen Energy*, 32 (2007) 4365-4380.
100. X.Z. Yuan, J.C. Sun, H. Wang, J. Zhang, *Journal of Power Sources*, 161 (2006) 929-937.
101. H.A. Gasteiger, W. Gu, R. Makharia, M.F. Mathias, B. Sompalli, "Handbook of Fuel Cells: Fundamentals, Technology, and Applications", Vol. 3, Wiley, 2003, p. 593, Chapter 46.
102. T.E. Springer, T.A. Zawodzinski, S. Gottesfield, *Journal of Electrochemical Society*, 138 (1991) 2334-2342.
103. D.R. de Sena, E.A. Ticianelli, E.R. Gonzalez, *Journal of Electroanalytical Chemistry*, 357 (1993) 225-236.
104. S.Y. Cha, W.M. Lee, *Journal of Electrochemical Society*, 146 (1999) 4055-4060.
105. H.-N. Su, S.-J. Liao, T. Shu, H.-L. Gao, *Journal of Power Sources*, 195 (2010) 756-761.
106. G. Sasikumar, J.W. Ihm, H. Ryu, *Electrochimica Acta*, 50 (2004) 601-605.
107. G. Sasikumar, J.W. Ihm, H. Ryu, *Journal of Power Sources*, 132 (2004) 11-17.
108. A. Caillard, C. Charles, D. Ramdutt, R. Boswell, P. Brault, *Journal of Physics D: Applied Physics*, 42 (2009) pp. 9.
109. C. Yang, S. Srinivasan, A.B. Bocarsly, S. Tulyani, J.B. Benziger, *Journal of Membrane Science*, 237 (2004) 145-161.